HHS Public Access

Author manuscript

Brain Behav Immun. Author manuscript; available in PMC 2023 September 12.

Published in final edited form as:

Brain Behav Immun. 2023 January ; 107: 16–31. doi:10.1016/j.bbi.2022.09.014.

Early life stress impairs synaptic pruning in the developing hippocampus

Kiran K. Dayananda[1],

Sahabuddin Ahmed[1],

Daniel Wang,

Baruh Polis,

Rafiad Islam,

Arie Kaffman[*]

Department of Psychiatry, Yale University School of Medicine, 300 George Street, Suite 901, New Haven, CT 06511, USA

Abstract

Early life adversity impairs normal hippocampal function and connectivity in various mammalian species, including humans and rodents. According to the '*cumulative model*' the number of early adversities can be summed up to determine the risk for developing psychopathology later in life. In contrast, the '*dimensional model*' argues that '*Deprivation*' and '*Threat*' impact different developmental processes that should not be added in determining clinical outcomes. Here we examine these predictions in male and female mice exposed to a single adversity — limited bedding (LB) — versus mice exposed to multiple adversities — unpredictable postnatal stress (UPS) — focusing on microglia-mediated synaptic pruning in the developing hippocampus. Exposure to both LB and UPS reduced the ramification of microglia, impaired their ability to phagocytose synaptic material in vivo and ex vivo, and decreased expression of TREM2. Abnormal phagocytic activity was associated with increased spine density in CA1 pyramidal neurons that was seen in 17-day-old groups and persisted in peri-pubescent 29-day-old LB and UPS mice. Exposure to LB caused more severe impairment in microglial ramification and synaptic engulfment compared to UPS, outcomes that were accompanied by a UPS-specific increase in the expression of several genes implicated in synaptic pruning. We propose that despite being a single stressor, LB represents a more severe form of early deprivation, and that appropriate levels of hippocampal stimulation during the second and third weeks of life are necessary to support normal microglial ramification and synaptic pruning. Further, impaired synaptic pruning during

[*]Corresponding author at: Arie Kaffman, 300 George Street, Suite 901, New Haven, CT 06511, USA. arie.kaffman@yale.edu (A. Kaffman).

[1]These authors have made similar contributions to the paper.

Declaration of Competing Interest

The authors declare that they have no known competing financial interests or personal relationships that could have appeared to influence the work reported in this paper.

Appendix A. Supplementary data

Supplementary data to this article can be found online at https://doi.org/10.1016/j.bbi.2022.09.014.

this critical period of hippocampal development contributes to the abnormal hippocampal function and connectivity seen in UPS and LB later in life.

Keywords

Early life stress; Mice; Microglia; Synaptic pruning; Limited bedding and nesting; Hippocampus

1. Introduction

Early life stress (ELS) is a heterogeneous group of adversities that includes childhood neglect, maltreatment, poverty, systemic racism and exposure to high levels of violence or crime (Teicher and Samson, 2016; White and Kaffman, 2019). Exposure to ELS is now recognized as a major public health concern (Peterson et al., 2018) and an important risk factor for abnormal brain development (Teicher and Samson, 2016). Different subtypes of ELS (e.g., physical abuse vs emotional neglect) cause somewhat different neurodevelopmental and behavioral outcomes that are further modified by sex and the timing of the adversity. Further, most cases of ELS are characterized by a combination of several subtypes of maltreatments that interact with one another to modify the risk for future psychopathology, reviewed in (White and Kaffman, 2019).

One of the most robust clinical findings is that Individuals exposed to multiple adversities are at higher risk for developing a broad range of psychiatric and medical conditions compared to individuals exposed to a single adversity (Anda et al., 2006; Chen et al., 2010; Evans et al., 2013; Kessler et al., 1997; McLaughlin et al., 2020). These observations have led some to propose a '*cumulative risk model*' in which the number adversities is simply added to predict clinical outcomes later in life (Evans et al., 2013). Others have challenged this model and proposed a '*dimensional model*' in which adversities are grouped into two distinct dimensions: '*Threat*' on the X-axis and '*Deprivation*' on the Y-axis (Fig. S1). *Threat* relates to experiences of physical danger to self (e.g., physical abuse, neighborhood violence) whereas *Deprivation* is the absence of appropriate sensory, cognitive, or social stimulation during early development (e.g., neglect, severe poverty). According to the '*dimensional model*', *Threat* and *Deprivation* cause different developmental processes and thus cannot be simply added to predict clinical outcomes. For example, threat-related adversities are associated with changes in amygdala connectivity and increase amygdala activation in response to intimidating cues, whereas deprivation is more commonly associated with cortical thinning, hyperactivity, and cognitive deficits (McLaughlin and Sheridan, 2016; McLaughlin et al., 2014).

Despite the appeal and clinical support available for both models they have not been tested in animals (White and Kaffman, 2019). To address this question, we developed a rodent model that compares outcomes in mice exposed to no stress (control condition), a single stressor in the form of limited bedding (LB), and multiple unpredictable stressors (unpredictable postnatal stress, or UPS). The LB paradigm used here is a modification of a widely used rodent model of early adversity in which pups are raised with limited bedding and nesting material (Bolton et al., 2017; Walker et al., 2017). However, our LB

paradigm extends the stress period from postnatal day 0 (P0, or birth) to P25 instead of the more common stress period of P2-P9. This was done in order to assess the impact of LB on developmental processes seen in early childhood and adolescence such as myelination and synaptic pruning in cortical areas (Johnson et al., 2018; White et al., 2020; Workman et al., 2013; Zeiss, 2021). Mice exposed to UPS are exposed to LB (stressor 1) and six unpredictable episodes of 1hr maternal separation on P14, P16, P17, P21, P22, and P25 followed by nest disruption (stressors 2 and 3 respectively). This experimental setup was designed to determine how the addition of multiple and unpredictable stressors, during a developmental period in the mouse corresponding to early childhood and adolescence in humans (e.g., P14-25), alters developmental and behavioral outcomes later in life.

According to the cumulative model, UPS mice would be expected to show more severe outcomes across diverse behavioral and developmental measures. A similar pattern is also predicted by the dimensional model for threat-related developmental processes because rodent pups are entirely dependent on the dam for survival and maternal separation has been known for decades to induce a robust stress response in the pups (Kaffman and Meaney, 2007; Kuhn and Schanberg, 1998). However, according to the dimensional model, LB is likely to induce more severe impairments in deprivation-related processes because of the constant impoverished conditions imposed by the limited availability of soft nesting material and poor nesting quality (Kaffman and Meaney, 2007; White and Kaffman, 2019). In contrast, UPS pups are briefly exposed to human contact and allowed to freely explore a novel environment for 1hr, on six different occasions, during a period of accelerated motor, sensory and cognitive development, experiences that may represent a mild form of enrichment (Fig. S1).

Consistent with the predictions of both models, we have previously found increased anxiety like-behavior in juvenile and adult UPS mice compared to mice reared under control or LB conditions (Johnson et al., 2018), findings that were recently confirmed by others (Orso et al., 2020). Moreover, high-resolution diffusion magnetic resonance images found several structural changes in adult UPS mice that resemble those seen in humans exposed to complex trauma including, reduced prefrontal cortex volume, reduced corpus callosum/fractional anisotropy, increased amygdala size, abnormal fronto-limbic connectivity and changes in global connectivity such as small-worldness and global efficiency (White et al., 2020). These findings support the clinical utility of UPS as a rodent model of complex childhood trauma and a useful tool for comparing outcomes of multiple versus a single adversity in the mouse.

Here we examine the effects of LB and UPS on microglia-mediated synaptic pruning in the hippocampus of 17-day-old pups. We focused on this process because the hippocampus undergoes intense synaptic pruning at this age (Favuzzi et al., 2021; Filipello et al., 2018; Paolicelli et al., 0000; Scott-Hewitt et al., 2020; Zhan et al., 2014) and because both LB and UPS have been shown to cause long-term impairment in hippocampal dependent learning (Rocha et al., 2021; White et al., 2020). In addition, connectivity between the hippocampus and several other brain regions, including the amygdala and the prefrontal cortex, is regulated by microglia (Filipello et al., 2018; Zhan et al., 2014) and is increased in UPS mice (White et al., 2020). Exposure to LB reduces microglial ramification in

the developing hippocampus (Hoeijmakers et al., 2017; Johnson et al., 2018) raising the question of whether these morphological changes impact synaptic pruning, and whether similar changes are also seen in mice exposed to UPS. Finally, our imaging studies indicate that UPS increases fronto-limbic connectivity in adult males, but not in females (White et al., 2020), suggesting that UPS may affect male and female microglia differently.

2. Methods

2.1. Animals

BALB/cByj mice (Stock # 001026, Jackson Laboratories) were housed in standard Plexiglas cages and kept on a standard 12:12 h light–dark cycle (lights on at 07.00 AM), constant temperature and humidity (22 °C and 50 %) with food and water provided ad libitum. Studies involving Trem2 knockout mice (Jackson Laboratories, Stock # 027197) were conducted by mating heterozygous mice to generate mixed litters containing wildtype, heterozygous, and knockout littermates raised under control condition (see below). At P17, these mice were processed to assess ex vivo and in vivo phagocytic activity. All studies were approved by the Institutional Animal Care and Use Committee (IACUC) at Yale University and were conducted in accordance with the recommendations of the NIH Guide for the Care and the Use of Laboratory Animals.

2.2. Early life stress models

ELS procedures were done as described previously (Johnson et al., 2018). Briefly, Female and male BALB/cByj mice, 6–8 weeks old, were purchased from the Jackson Laboratory, housed five mice per cage in standard mouse Plexiglas cages layered with 500 cc of corncob bedding, but with no nesting material, and allowed to acclimate for 12 days in the animal facility. Mice were mated, using a 3:1 female to male ratio, in standard mouse Plexiglas cages layered with 500 cc of corncob bedding but with no nesting material. Visibly pregnant dams were transferred to ‘maternity cages’ containing 500 cc corncob bedding but no nesting material. At birth, postnatal day (P0) litters were culled to 5–8 pups and randomized to either control (CTL), limited bedding (LB), or unpredictable postnatal stress (UPS) conditions. Mice raised under CTL condition were provided with 500 cc of fresh corncob bedding, an additional 15 cc of soiled bedding from the original cage, and one 5 × 5 cm nestlet per cage. LB and UPS litters were provided with 125 cc of corncob, 15 cc of soiled bedding from the original cage, and no nesting material (Fig. 1A–B). UPS litters were also separated from their dam for one hour per day (10:00 AM–11:30 AM) on P14, P16, P17, P21, P22, P25. During the separation period, the dam was transferred to a new cage, followed by transferring the pups to a different cage containing clean corncob bedding and the empty home-cage was briefly shaken to evenly spread the bedding and disrupt the nest. At the end of the one-hour separation, the pups were returned to their home cage followed by the return of the dam (Fig. 1B). The bedding was changed weekly. Most pups were processed for tissue collection at P17, except for one cohort of mice (n = 36) that went through the entire procedure (P0-25). These mice were weaned on P26 and housed with 2–3 same sex and condition per cage until processed for Golgi at P29 (Fig. 5D).

2.3. Tissue collection

Tissue was collected between 11:00 and 13:00 to minimize the diurnal effects of corticosterone. Tissue collected at P17 from UPS pups was processed 5–30 min after reuniting with the dam. Pups were individually removed from the home cage with an effort made to minimally disturb the dam and the other littermates and placed in a standard plexiglass cage layered with fresh bedding and 50 cc of soiled bedding. For tissue collection involving perfusion, blood collection, and microglia characterization, pups were first anesthetized with chloral hydrate (100 mg/kg) and, when sedated, transferred to a nearby procedural room for tissue collection. Tissue collection for Golgi staining, synaptosome preparation, and blood collection was done by acute decapitation in the procedural room.

2.4. Corticosterone assessment

Pups were rapidly decapitated, and blood was collected in heparinized tube, spun at 5000×*g* for 5 min at r.t and stored as plasma at − 80 °C for later analysis. Plasma corticosterone levels were determined using ELISA in duplicates (Cat. # K014-H1, Arbor Assays, Ann Arbor, MI).

2.5. Immunohistochemistry

Mice were anesthetized with chloral hydrate (100 mg/kg) and transcardially perfused with ice-cold PBS/heparin (50 u/ml) solution followed by 10 % formalin. Brains were then post-fixed for 72 hrs at 4 °C in 10 % formalin and then sliced using a VT1000S vibratome (Leica). Forty-micron coronal sections were collected in 6 pools, each containing16-18 slices, spanning the entire rostral-caudal axis of the hippocampus. Morphological analysis was done by incubating one pool of slices with rabbit anti Iba1 1:1000 (Wako, Cat. #019-19741) overnight at 4 °C. To assess PSD95 and CD68 staining, a second pool of slices was incubated with rabbit anti Iba1 1:500 (Wako, Cat. #019-19741), PSD95 1:100 (Merck-Millipore, Cat. # MAB1596), and CD68 1:400 (BioRad, Cat. # MCA1957T), followed by fluorescently labeled secondary antibodies (ThermoFisher, 1:400). Stained slices were then mounted on glass slides with VECTASHIELD HardSet antifade mounting medium with DAPI (Vector laboratories Cat# 10955).

2.6. Microscopy and morphological analysis

Iba1 positive cells localized to the CA1, and DG regions of the dorsal and ventral Hippocampus were imaged using FluoView 1000 confocal microscope (Olympus). Three independent Z-stacks measuring 212 μm (W) × 212 μm (L) × 25 μm (D) were obtained for each brain region using 1um intervals. Image analysis was done with ImageJ/FIJI (NIH) software using analyze skeleton2D/3D plugin using the following protocol. Eight-bit grayscale images were generated to best visualize all positive staining and the Unsharp Mask filter was run to further increase contrast. Despeckle step was then used to remove salt-and-pepper noise generated by the Unsharp Mask. Images were then converted to binary and characterized using the plugin AnalyzeSkeleton (2D/3D) checking the Branch Information box. Results were pasted into an Excel spreadsheet to obtain average branch length and endpoint voxels per microglial cell. Outcomes from the 3 images were then averaged to obtain a single value for each animal.

To assess PSD95 and CD68 staining inside microglia, Z-stacks images in the dorsal stratum radiatum region of the hippocampus were collected with an LSM-880 Airyscan confocal microscope (Zeiss) equipped with a plain Apochromat 63x/1.4 oil DIC M27 objective. For each region, 5–6 fields of view were acquired by a Zen Blue 2.1 software (Zeiss), zoom factor 2, fixed frame size of 67.5 μm × 67.5 μm in XY plain, z-step size of 0.30 μm, for a total thickness of 12–15 μm. Images were deconvoluted with Zen Black software and were processed and analyzed using the 3D surface rendering software Imaris version-9.7.2 (Oxford Instruments, Abingdon, United Kingdom). Briefly, A ROI (45 μm × 45 μm × 10 μm) was selected using the cropped function to create 3D reconstruction surfaces in each channel using a semi-automated threshold, fixed voxel, and automated background subtraction. PSD95 puncta were detected and measured using the spot function with a threshold of 0.3 μm. Iba-1 and CD68 volumes were calculated algorithmically using the surface function in Imaris. The number of PSD95 puncta and $CD68^+$ phagolysosomes engulfed within $Iba1^+$ surfaces were counted using the 'spot closed to surfaces' function with a threshold set at zero. Iba1 volume, CD68 volume inside microglia, PSD95 puncta inside microglia, and PSD95 puncta inside CD68 were averaged across 5–6 microglia cells examined per animal, and these averages were used for the analysis. Values from all cells were used to assess the Pearson correlation between microglia volume and PSD95 puncta or CD68 volume inside microglia (Fig. S3).

2.7. Synaptosomal preparation and labeling with pHrodo dye

P21 Balb/cByj pups raised in the vivarium were anesthetized with chloral hydrate (100 mg/kg) and the hippocampus was dissected out and placed in a 2-ml Dounce homogenizer (Kimble Chase) containing 500 μl of ice-cold buffer A [HEPES 4 mM pH 7.4, 320 mM sucrose, 1 mM DTT, and protease inhibitor cocktail (cat. No. P2714, Sigma)] and homogenized sequentially using plunger A (5 S) and plunger B (5 S). The homogenate was transferred into a cold Eppendorf tube and centrifuged for 5 min at 1000 g at 4 °C to remove nuclei and cell debris (P1 fraction). The supernatant was transferred to a new Eppendorf tube and centrifuged for 20 min, 15,000g, at 4 °C. The supernatant containing soluble proteins was transferred to a new Eppendorf tube (S2) and snap frozen in liquid nitrogen. The remaining pellet (P2 fraction), containing the crude synaptosomes was stained with pHrodo green (Thermo Fisher P36013) using 1:10 protein:dye molar ratio and resuspended at 1 mg/ml concentration in 5 % DMSO in buffer A and frozen at −80 °C freezer until further used for phagocytosis assay (Fig. S4).

2.8. Ex-vivo phagocytic assay

Microglia were purified from P17 developing hippocampus using a Percoll gradient as described previously (Delpech et al., 2016). In brief, pups were anesthetized with chloral hydrate (100 mg/kg) and both hippocampi were dissected and homogenized in 2 ml of cold HBSS using a glass tissue homogenizer (Kimble Chase) using plunger A followed by plunger B (5 S for each plunger). Homogenates were then transferred into a 15 ml Falcon tube, diluted with 10 ml of ice-cold HBSS, and spun (280 g, 4 °C) for 7 min. The supernatant was decanted, and the cell pellet was resuspended in 5 ml of 70 % Percoll solution layered with additional 5 ml of 37 % Percoll solution. Cells were spun at 800 g for 25 min at 20 °C (brake off), and microglia-enriched fraction was collected from the 70

%/37 % interphase. Microglia-enriched fraction was then washed with 10 ml of cold FACS buffer (0.2 % BSA in HBSS), and spun at 280 g for 7 min at 4 °C. The supernatant was removed, and the cell pellet was resuspended in RPMI/1% BSA buffer, and divided into two aliquots, each containing approximately 50,000 microglia. Each aliquot was incubated with 60 μl of labeled synaptosomes (1 mg/ml concentration) in a total reaction volume of 400 μl RPMI/1% BSA buffer and kept at 37 °C and 5 % of CO2 for 40 min. Reactions were stopped by the addition of cold RPMI/1% BSA buffer and placed on ice. Cells were then pelleted at 2000 rpm for 10 min at 4 °C, resuspended in 200 μl of RPMI/1%BSA buffer, stained with CD11b-PE Cy7 and CD45-PeCPCy5.5 antibodies and processed for FACS analysis. Microglia cells without labelled synaptosomes were used for gating baseline to calculate the percentage of phagocytic cells (Fig. S4).

2.9. Golgi staining and morphological analysis

Golgi staining and analysis were done as previously described (Wei et al., 2015; Wei et al., 2012). Briefly, P17 and P29 mice were weighed and rapidly decapitated. Brains were then carefully removed, and the left hemispheres stained for 8d using the FD Neurotechnologies Rapid GolgiStain™ kit. Impregnated hemispheres were snap-frozen in isopentane/dry ice bath and stored at −80 °C. Frozen hemispheres were then cut into 150-μm sagittal sections using a cryostat, mounted onto gelatin-coated slides (FD Neurotechnologies, Cat # PO101), stained, and cover-slipped for bright field microscope imaging. Stained slides were coded to ensure that morphological analysis was conducted by an observer who was blind to the animal's sex and developmental history. CA1 pyramidal cells in the dorsal hippocampus that were fully impregnated and free of neighboring cells or cellular debris were randomly selected for imaging and analysis (n = 5 cells per animal). Cells were traced using Neurolucida 10.0 software (MBF Bioscience), and soma size, total branch length (summing both apical and basal dendrites), and the number of branch endpoints were calculated. Spine density for each neuron was determined by averaging densities obtained from 3 tertiary dendritic segments (about 15–20 μm each) for 15 dendritic segments per animal.

2.10. Flow cytometry to assess receptor expression on microglia

Microglia were isolated from the hippocampus as described above and blocked with rat-anti CD16/CD32 Fc antibodies 1:100 (Cat# 553142, BD Biosciences) and then stained with rat-anti CD11b-PeCy7 1:100 (Cat# 25-0112-82, ebiosciences), rat-anti CD45-PeCPCy5.5 antibodies 1:100 (Cat# 45-0451-82, ebiosciences), APC-rat anti Trem2 antibodies 1:10 (Cat# FAB17291A R & D systems), or APC-mouse anti CX3CR1 antibodies 1:100 (Cat# 149008) for 25 min on ice. Labeled cells were washed with 3 ml of cold FACS buffer, spun as above, resuspended in 300ul of cold FACS buffer and assessed for antigen expression using a BD LSR fortessa FACS (BD Biosciences). Data were analyzed using FlowJo software (Tree Star) and gating for each antibody was determined with isotype-stained control.

2.11. Microglia isolation for genomic studies

Microglia were isolated using the Percoll gradient and washed with cold FACS buffer as described for the ex vivo phagocytic assay except that cell pellet was resuspended in 300 μl of cold FACS buffer and blocked with rat- anti CD16/CD32 Fc antibodies 1:100

(Cat# 553142, BD Biosciences) and live/dead stain (Cat. #34965, Thermo Fisher) for 10 min on ice. Microglia were then stained with rat-anti CD11b-PeCy7 antibodies 1:100 (Cat# 25-0112-82, ebiosciences) and rat-anti CD45-PeCPCy5.5 antibodies 1:100 (Cat# 45-0451-82, ebiosciences) for 25 min on ice. Labeled cells were washed with 3 ml of cold FACS buffer, spun as above, resuspended in 300ul of cold FACS buffer and sorted using BD FACSAria™ II flow cytometer (BdBiosciences). Sixty thousand CD11b+, CD45 ^{low} cells were collected per sample and spun down at 400 g for 8 min at 4 °C. The supernatant was discarded, and the pellet resuspended in 5ul of 1/3RLT buffer (cat. No. 79216, Qiagen) and frozen at —80 °C until further genomic analysis using the mouse Glia panel (Nanostring, Cat. # XT-Mm Glial profiling CSO). Five μl of lysate were used for hybridization setup (65 °C for 16hrs) and mRNA counting using the nCounter manufacturer protocol. Samples from 8 pups (from 4 to 5 independent litters) per rearing and sex group were run in 4 batches of 12 reactions each (total of 48 reactions).

2.12. Nanostring analysis

Counts were normalized using all 13 housekeeping genes available on the mouse Glia panel and genes with counts greater than negative control (>20) were considered present. Preliminary MANOVA analysis of the 524 expressed genes revealed that most of the differentially regulated genes (DRGs) were regulated by rearing (87 DRGs) with relatively few genes regulated by sex (13 DRG) and only 5 DRGs showing significant interaction between rearing and sex. Based on the prominent rearing effect, advanced-analysis was conducted using the nSolver software (NanoString) to identify DRG between CTL and LB group, CTL and UPS, and LB and UPS with batch as a covariance to correct for differences noted in one of the batches used in this experiment. Ingenuity Pathway Analysis (IPA) (Qiagen) was used to assess the effects of LB and UPS on canonical pathways and transcription factor regulators using “user data setting” to account for the biased selection of genes of interest on the Glia panel. All data, including raw counts, were deposited and are available at: https://www.ncbi.nlm.nih.gov/geo/query/acc.cgi?acc=GSE190427.

2.13. C-fos mapping

Perfused brains from P17 pups were sectioned coronally using a sliding freezing microtome to obtain 40-μm sections, sorted into 6 pools, each containing 16–18 slices spaced at 240-μm intervals that systematically span the entire rostral-caudal axis of the brain. One pool of slices was incubated at 4 °C overnight with rabbit anti-c-fos (Cat. # 2250, Cell Signaling), followed by anti-rabbit biotinylated secondary antibody (Vector Labs, 1:250) and visualized with the ABC kit (Vector Labs) and 3′,3′ diaminobenzidine (DAB) staining. Slices were then dried overnight and counterstained with Hematoxylin stain (Vector Labs). An average of 6 slices containing the left and right hippocampi were present in each pool and were used to count c-fos positive cells from the entire CA1, CA2 and CA3 sub-regions under 20x magnification by a researcher blind to sex and experimental condition. The total number of c-fos positive cells present in the entire hippocampus was calculated by adding up the number of c-fos-positive cells counted for each animal and multiplying by 6 to account for sampling only one sixth of the hippocampus.

2.14. Statistical analysis

Data were carefully screened for inaccuracies, outliers, normality and homogeneity of variance using SPSS (IBM Corp. version 26) and visualized with GraphPad Prism (iOS, version 9.1.0). Data for microglial density, morphology, synaptic engulfment in vivo, and ex vivo phagocytic activity were analyzed using a two-way ANOVA examining the main effects of rearing (CTL, LB, UPS), sex, and their interaction. Significant interactions were followed by Tukey-HSD post-hoc analysis for each sex. Similar 3 × 2 ANOVA was used to assess the effects of rearing and sex on soma size, dendritic arborization and spine density in CA1 pyramidal neurons. One-way ANOVA was used to assess the effect of *Trem2* genotype on phagocytic activity with significant main effect followed by Tukey-HSD post-hoc analysis. For Nanostring, DRG were identified using two-sided *t*-test ($p < 0.05$) and Benjamini-Hochberg (B-H) correction for multiple Testing p-adj < 0.1). IPA analyses were done using the multiple comparisons feature with $Z > 1.5$ and $p < 0.05$.

3. Results

3.1. Plasma corticosterone levels are elevated in P17 UPS pups

The main effects of rearing condition (CTL, LB, UPS), sex, and their interaction on body weight and corticosterone levels were assessed in P17 pups (Fig. 1A for timeline). This age was chosen to detect emerging differences in microglia function when the hippocampus undergoes intense synaptic pruning (Favuzzi et al., 2021; Filipello et al., 2018; Paolicelli et al., 0000; Scott-Hewitt et al., 2020; Zhan et al., 2014). Moreover, we have previously found reduced microglial ramification in 14-day-old LB pups (Johnson et al., 2018) and wanted to test whether exposure to three unpredictable episodes of maternal separation and nest disruption would reveal differences in microglial activity between LB and UPS pups (Fig. 1A–B). Consistent with our previous work (Johnson et al., 2018; White et al., 2020), we found reduced weight in LB and UPS pups compared to control (CTL) P17 pups, with no significant effect of sex or interaction (rearing: $F(2, 42) = 6.45$ $P = 0.0036$, sex: $F(1, 42) = 0.30$ $P = 0.58$, interaction: $F(2, 42) = 0.36$ $P = 0.70$). Tukey-HSD post-hoc analysis showed a significant reduction in weight between CTL-LB ($P = 0.0035$) and CTL-UPS ($P = 0.037$) and no difference in body weight between LB and UPS ($P = 0.64$, Fig. 1C). There was a significant main effect of rearing on plasma corticosterone ($F(2, 29) = 3.705$, $P = 0.037$, $\eta_p^2 = 0.095$) that was seen in both males and females and was driven by a significant increase in corticosterone levels in UPS compared to CTL ($P = 0.030$, Cohen's $d = 0.75$), with LB showing intermediate levels that were not significant when compared to CTL ($P = 0.58$) or UPS ($P = 0.21$, Fig. 1D). These findings suggest that UPS further exacerbates the mild distress seen in LB pups.

3.2. LB causes more pronounced reduction in microglial ramification compared to UPS

Next, we assessed the effects of rearing, sex and their interaction on microglial density and morphology in 4 sub-regions of the hippocampus: 1) dorsal hippocampus CA1 (dHP-CA1), 2) dorsal hippocampus dentate gyrus (dHP-DG), 3) ventral hippocampus CA1 (vHP-CA1), and 4) ventral hippocampus dentate gyrus (vHP-DG). Microglia were stained with Iba1 antibodies and imaged with confocal microscopy as described in the Methods section. Inspection of the images revealed reduced ramification in mice exposed to LB and to a lesser

degree in UPS mice compared to CTL (Fig. 2A). Table S1 provides a detailed summary of the density and morphological analyses. A 3 X 2 ANOVA found no significant effects of rearing, sex or interaction for microglial density in these 4 brain regions (Supplemental Information Fig. S2). There was a significant effect of rearing with a large effect size on microglial branch length in the dHP-CA1 ($F (2, 25) = 9.70$, $P = 0.0008$, $\eta_p^2 = 0.49$, Fig. 2B) with no significant effects of sex or interaction. Tukey-HSD post-hoc analysis revealed a significant reduction in branch-length in LB ($P = 0.0006$) and UPS ($P = 0.017$) compared to CTL mice, with no difference between LB and UPS ($P = 0.27$). A significant rearing effect was also seen in the dHPC-CA1 for the number of branch-endpoints per microglia $F (2, 25) = 5.54$, $P = 0.010$, $\eta_p^2 = 0.31$) with no significant effects of sex or interaction (Fig. 2C). Follow-up post hoc analysis found reduced number of branch endpoints in LB ($P = 0.0077$) but not UPS ($P = 0.11$) compared to CTL animals, and no difference between LB and UPS ($P = 0.37$). Similar pattern was seen in the dHPC-DG, with a large main effect for rearing condition for branch length $F (2, 25) = 9.70$, $P = 0.0008$, $\eta_p^2 = 0.35$) and no significant effects of sex or interaction (Fig. 2D). The rearing effect was due to reduced branch length in LB ($P = 0.0006$) and UPS ($P = 0.017$) compared to CTL condition, with no difference between LB and UPS ($P = 0.27$). There was also a significant rearing effect in the number of branch-endpoints in the dHPC-DG ($F (2, 25) = 6.23$, $P = 0.0064$, $\eta_p^2 = 0.33$) with reduced number of branch endpoints in LB compared to CTL ($P = 0.011$) and UPS ($P = 0.018$) with no difference between UPS and CTL ($P = 0.91$). There was no significant main effect of sex or interaction for the number of branch endpoints in the dHPC-DG (Fig. 2E).

In the ventral hippocampus CA1 region, a 3 X 2 ANOVA found significant rearing effect for branch length ($F (2, 23) = 4.83$, $P = 0.018$, $\eta_p^2 = 0.30$) with no significant effect of sex or interaction. Follow-up post-hoc analysis showed reduced branch length in LB compared to CTL ($P = 0.013$) but no other significant differences between the groups (Fig. 2F). There was no significant main effect of rearing, sex or interaction for the number of microglial endpoints in the vHPC-CA1 (Fig. 2G). A significant effect of rearing was also found for branch length in vHPC-DG ($F (2, 23) = 5.28$, $P = 0.013$, $\eta_p^2 = 0.32$) driven by reduced branch length in LB compared to CTL ($P = 0.031$) and UPS ($P = 0.024$), with no significant difference between CTL and UPS (Fig. 2H). A trend for a rearing effect was seen for the number of endpoints in the vHPC-DG ($F (2, 23) = 3.19$, $P = 0.060$, $\eta_p^2 = 0.22$, Fig. 2I). No significant effects of sex or interaction were found for branch length (Fig. 1H) or the number of endpoints (Fig. 2I) in the vHPC-DG (Table S1).

Since LB and UPS pups are smaller than CTL pups and microglial ramification in the hippocampus increases with age (Delpech et al., 2016), we sought to clarify whether body weight mediated the effects of LB and UPS on branch length and the number of endpoints. Pearson correlation between weight and branch length revealed no significant correlation between body weight and branch length or number of endpoints for any of the brain regions examined (Table S1A). In addition, significant rearing effects were still seen after using weight as a covariance in the 2 × 3 ANOVA (Table S1B). In summary, exposure to LB and UPS caused a significant reduction in microglial ramification that was not due to reduced body weight and was not associated with changes in microglial density. Reduced microglial ramification in the developing hippocampus was more pronounced in LB compared to UPS

pups, revealing potentially interesting changes in microglial function between these two models of ELS.

3.3. Reduced microglial volume is correlated with abnormal engulfment of synaptic material in vivo

To clarify the physiological impact of reduced microglial ramification on their ability to phagocytose synaptic material, we used an independent cohort of P17 pups to assess the effects of rearing and sex on microglial volume (Iba1 staining), phagosome volume (CD68 staining) and the number of PSD95 puncta located inside microglia. Consistent with our initial observations, we found a significant rearing effect on microglial volume ($F(2, 22) = 112.7$, $P < 0.0001$, $\eta_p^2 = 0.9$, Fig. 3A–B). Tukey-HSD post-hoc analysis indicated a significant reduction in microglial volume in LB ($P < 0.0001$, Cohens d = 5.92) and UPS ($P < 0.0001$, Cohens d = 4.9) compared to the CTL group. UPS microglia were larger ($878 \pm 52\ \mu m^3$) compared to LB microglia ($659 \pm 65\ \mu m^3$), with a large effect size (Cohen's d = 1.19), but this difference did not reach significance after adjusting for multiple comparisons ($P = 0.15$, Fig. 3B). Similar pattern was seen for CD68 volume (rearing: $F(2, 22) = 28.45$, $P < 0.0001$, $\eta_p^2 = 0.73$, Fig. 3C), number of PSD95 puncta inside microglia (rearing: $F(2, 22) = 27.03$, $P < 0.0001$, $\eta_p^2 = 0.70$, Fig. 3D), and the number of PSD95 puncta inside CD68 (rearing: $F(2, 22) = 23.28$, $P < 0.0001$, $\eta_p^2 = 0.77$, Fig. 3E). Post-hoc analyses found a significant reduction in CD68 volume and PSD95 puncta in LB and UPS groups compared to CTL (Fig. 3C–E). There was a consistent increase in these measurements in UPS compared to LB, but these differences did not reach significance for CD68 volume (CTL vs UPS $P = 0.16$, Cohen's d = 1.24, Fig. 3C) and the number of PSD95 inside microglia (CTL vs UPS $P = 0.17$, Cohen's d = 1.37, Fig. 3D). However, there was a significant difference between UPS and LB for the number of PSD95 puncta inside CD68 ($P = 0.038$, Cohen's d = 7.29, Fig. 3E). No significant effects of sex or interaction between sex and rearing were found for microglia volume, CD68 volume, and the number of PSD95 in microglia and in the CD68 compartment within microglia.

The total number of PSD95 puncta outside microglia was similar in all three groups ($F(2, 18) = 0.67$, $P = 0.52$, Fig. S3A) indicating that these outcomes were not driven by a reduction in PSD95 availability. Instead, the volume of microglia was highly correlated with CD68 volume ($r = 0.67$, $P < 0.0001$, Fig. S3B), PSD95 puncta inside microglia ($r = 0.86$, $P < 0.0001$, Fig. S3C) and PSD95 puncta inside CD68 ($r = 0.67$, $P < 0.0001$). Similarly, normalizing CD68 volume or the number of PSD95 puncta inside microglia to microglial volume eliminated differences between CTL, LB and UPS (Fig. S3D–E). Together, these findings suggest that reduced microglial volume in LB and UPS P17 pups plays an important role in impairing their capacity to internalize synaptic material in the developing hippocampus.

3.4. ELS impairs microglial phagocytotic activity ex vivo

Next, we assessed the effects of rearing, sex and their interaction on the ability of acutely purified microglia to phagocytose pHrodo-labeled synaptosomes (See Fig S4 for details). Using this ex vivo phagocytic assay we found a significant rearing by sex interaction ($F(2, 111) = 3.57$, $P = 0.031$, $\eta_p^2 = 0.06$). Follow-up Tukey-HSD post-hoc analysis in males,

revealed a significant reduction in phagocytic activity in LB (P = 0.0002) and UPS (P = 0.0002) compared to CTL, with no difference between LB and UPS (P = 0.95, Fig. 4E). In females, LB microglia showed a significant reduction in phagocytic activity compared to CTL (P = 0.0001). However, unlike UPS males that were indistinguishable from LB males, UPS females had intermediate levels of phagocytic activity that was significantly higher compared to LB (P = 0.0017), but lower compared to CTL females (P = 0.019). Together, these findings reveal a significant impairment in the ability of LB and UPS microglia to phagocytose synaptosomes, a deficit that appears to be more modest in UPS females.

3.5. ELS increases spine density in CA1 pyramidal neurons in P17 and P29 mice

Abnormal microglia-mediated synaptic pruning has previously been shown to increase spine density in the developing hippocampus (Filipello et al., 2018; Paolicelli et al., 2011; Schafer et al., 2012; Scott-Hewitt et al., 2020; Zhan et al., 2014). To test whether this is also the case in LB and UPS mice, we used Golgi staining to assess spine density and dendritic arborization in CA1 pyramidal neurons of P17 pups (Fig. 5A). There were no significant effects of rearing, sex or interaction on soma size, number of dendritic endpoints, and dendritic length (Fig. S5). However, there was a significant effect of rearing on spine density ($F (2, 24) = 7.54$, $P = 0.0029$, $\eta_p^2 = 0.39$) (Fig. 5B–C) with no significant effect of sex ($F (1, 24) = 2.83$, $P = 0.11$) or interaction ($F (2, 24) = 0.51$, $P = 0.61$). Post-hoc analysis revealed a significant increase in spine density in LB compared to CTL ($P = 0.0032$) and between UPS and CTL ($P = 0.021$), with no difference between LB and UPS ($P = 0.71$). There was no significant correlation between body weight and spine density ($r = -0.189$, $P = 0.33$, $n = 29$) indicating that the increase in spine density was not likely due to lower body weights in LB and UPS pups.

Next, we repeated the Golgi analysis in P29 when spine density in the hippocampus reaches adult-like levels (Grossman et al., 2010; Paolicelli et al., 2011) and the mice are no longer exposed to LB or UPS. Similar to findings at P17, there was a significant effect of rearing with a large effect size on spine density ($F (2, 24) = 19.56$, $P < 0.0001$, $\eta_p^2 = 0.62$, Fig. 5D) that was due to reduced spine density in CTL compared to LB ($P < 0.0001$) and UPS ($P < 0.0001$) with no difference between LB and UPS ($P = 0.99$). There was a marginal effect of sex ($F (1, 24) = 4.03$, $P = 0.056$) and no significant interaction ($F (2, 24) = 1.73$, $P = 0.19$). As in P17, there were no significant effects of rearing, sex, or interaction on soma size, dendritic length, and number of endpoints at P29 (Fig. S5). Together, these findings are consistent with the notion that impaired microglial mediated phagocytic activity leads to increased spine density that is detected at P17 and persists in P29 mice.

3.6. LB and UPS cause complex and opposing changes in the expression of receptors that mediate synaptic pruning

To clarify the mechanisms by which LB and UPS impair synaptic pruning, we isolated hippocampal microglia from P17 and used flow cytometry to quantify surface expression of TREM2, CD11b/complement C3 receptor, and CX3CR1; microglial receptors that have been shown to guide synaptic pruning in the developing hippocampus (Filipello et al., 2018; Paolicelli et al., 2011; Schafer et al., 2012; Scott-Hewitt et al., 2020; Zhan et al., 2014). We found that roughly 60 % of P17-CTL microglia express TREM2 (Fig 6A–B) and that

the percentage of TREM2-positive microglia was significantly reduced in LB and UPS pups (main effect of rearing.

(F (2, 71) = 17.47, P < 0.0005, post-hoc CTL-LB (P= <0.0001), CTL-UPS (P= <0.0001). There was no significant effect of sex (F (1, 71) = 0.084, P = 0.77) or interaction (F (2, 71) = 0.084, P = 0.92) and no difference between LB and UPS groups (P = 0.83, Fig. 6A–B). Similar outcomes were seen when mean fluorescence intensity (MFI) was used to assess surface levels of TREM2 (Fig. S6A–B). No differences in levels of *Trem2* mRNA were seen in microglia isolated from the developing hippocampus of CTL, LB and UPS pups (Fig. S6C), suggesting that TREM2 protein levels are regulated at the post-transcriptional level.

CD11b surface expression showed a significant interaction between rearing and sex (F (2, 52) = 3.50, P = 0.037) that was due to reduced levels in LB males (P = 0.0029) and UPS males (P = 0.0003) compared to CTL males, with no difference between LB and UPS (P = 0.78). No differences in CD11b levels were seen between the groups in females (Fig 6 C–D). CD45 levels were significantly lower in UPS compared to LB (P = 0.0050) and CTL (P = 0.0003) with no difference between LB and CTL (P = 0.85, Fig. 6 E–F). Surprisingly, levels of CX3CR1 protein were highest in UPS followed by LB and lowest in CTL (rearing: F (2, 57) = 21.65, P < 0.0001, LB vs CTL (P = 0.0055), LB vs UPS (P = 0.0068), an effect that was seen in both males and females (Fig. 6 G–H). Together, these findings reveal complex changes in levels of receptors that mediate synaptic pruning in microglia isolated from the hippocampus of LB and UPS pups.

3.7. Trem2 is necessary for normal phagocytic activity

Since TREM2 levels are reduced in both LB and UPS male and female mice and *Trem2* knockout mice show reduced capacity to engulf synaptic material and increased spine density in CA1 neurons (Filipello et al., 2018; Scott-Hewitt et al., 2020), we isolated microglia from the hippocampus of P17 Trem2-wildtype (WT), Trem2-heterozygous (Hets), and Trem2-knockout (Ko) littermates and tested their ability to engulf pHrodo-labeled synaptosomes ex vivo. We found a dose-dependent effect of genotype (F (2, 36) = 8.92, P = 0.0007) with WT showing the highest ex vivo phagocytic activity followed by Hets and microglia from *Trem2* KO mice showing the lowest ex vivo phagocytic activity (Fig. 7A–B). Next, we tested the effects of Trem2 genotype on microglial volume, CD68 volume, and PSD95 engulfment in vivo. There was a significant effect of genotype on microglial volume (F (2, 12) = 12.1, P = 0.0021) that was due to increased volume in *Trem2*-WT microglia compared to *Trem2*-ko microglia (P = 0.0016), with *Trem2*-hets showing an intermediate phenotype (Fig. 7C–D). Significant effect of genotype was also seen for CD68 volume (F (2, 12) = 7.98, P = 0.0085, Fig. 7E), number of PSD95 puncta inside microglia (F (2, 12) = 25.9, P = 0.0001, Fig. 7F), and PSD95 puncta inside CD68 (F (2, 12) = 16.6, P = 0.0007, Fig. 7G). No significant effects of sex or interaction were found for the ex vivo and in vivo phagocytic activities tested. These findings confirm previous work (Filipello et al., 2018; Scott-Hewitt et al., 2020), and suggest that reduced TREM2 levels contributes to the abnormal phagocytic activity seen in LB and UPS P17 pups.

3.8. UPS causes distinct transcriptional changes compared to LB and CTL groups

Next, we used the mouse Glia panel to identify differentially regulated genes (DRG) in microglia isolated from the hippocampus of 17-day-old pups. Preliminary 3 × 2 MANOVA analysis of the 478 genes detected by the panel (>20 counts) found few DRG with a significant main effect of sex or interaction (Table S2). Therefore, we focused on rearing effects among the three different conditions. Using this approach, we found 56 DRG in LB compared to CTL ($p < 0.05$ uncorrected for multiple comparisons, Fig. 8A). No DRG were found between CTL and LB after Benjamini-Hochberg correction for multiple comparisons (padj < 0.1, Fig. S7A and Table S3). The top 10 upregulated and downregulated DRG in LB-CTL comparison are listed in Fig. 8B (left) and include upregulation of genes such as Marker of Proliferation Ki67 (*Mki67*), a marker of mitotically active microglia, and several cytokines including Tumor Necrosis Factor (*Tnf*) and Chemokine (C—C motif) Ligand 12 (*Ccl12*). Examples of downregulated genes in LB microglia included the neurotrophic factor Nerve Growth Factor (*Ngf*), *Cd34*, and the mitochondrial gene Translocator Protein (*Tspo*). For a complete list of all DRG between CTL and LB see Table S3.

Comparison between UPS and CTL conditions revealed 78 DRG ($p < 0.05$ uncorrected for multiple comparisons, Fig. 8A), with 34 DRG after adjusting for multiple comparisons (padj < 0.1, Fig. S7B and Table S3). Some of the most upregulated genes in UPS included the Adrenoceptor Beta 1 (*Adrβ1*), Toll Like Receptor 7 (*Tlr7*), Transmembrane Protein 119 (*Tmem119*), and the inflammasome component NLR Family Pyrin Domain Containing 3 (*Nlrp3*, Fig. 8B-middle). Examples of genes that were downregulated in UPS compared to CTL included G Protein-Coupled Receptor 84 (*Gpr84*), Killer Cell Lectin Like Receptor D1 (*Klrd1*) and Interleukin 1 Beta (Il1-*β*) (Fig. 8B-middle).

Ninety DRG were found between LB and UPS ($p < 0.05$ uncorrected, Fig. 8A), with 49 DRG significant at padj < 0.1 (Fig. S7C and Table S3). Several of the DRG in UPS-CTL comparison were also differentially regulated in the LB-UPS comparison (e.g. upregulated: *Adrβ1*, *Tlr7*, Kit Ligand (*Kitl1*), *Tmem119*, and Neutrophil Cytosolic Factor 1 (*Ncf1*), downregulated: *Il1-β*, *Gpr84*, Interleukin 21 Receptor (*Il21r*), Solute Carrier Family 12 Member 2 (*Slc12a2*). Genes that were upregulated in the LB-UPS comparison but not CTL-UPS comparison include: *Tspo*, Chondroitin Sulfate Proteoglycan 4 (*Cspg4*), Ankyrin 2 (*Ank2*), and Plexin B3 (*Plxnb3*). Examples of uniquely downregulated genes in UPS compared to LB include Interleukin 1 Alpha (*Il1-α*), Tripartite Motif Containing 17 (*Trim17*), Transmembrane 4L Six Family Member 1 (*Tm4sfM1*), and Signal Transducer and Activator of Transcription 1 (*Stat1*). Using an independent cohort of mice, we confirmed changes in 14 of 25 (70 %) of the DRG with additional 4 genes (20 %) showing a similar trend (Fig. S8).

UPS increased transcripts of several genes that promote synaptic pruning including complement C1q peptides (e.g., *C1qa, C1qb, C1qc*), MER Proto-Oncogene Tyrosine Kinase (*Mertk*), Signal Regulatory Protein Alpha (*Sirp α*), and several Toll Like Receptors (*Tlr7, Tlr4*) when compared to LB and CTL groups (Fig. 8C). The expression of several trophic factors and cytokines were also significantly different between LB and UPS including *1Ll-β, Tnf*, and Ngf (Fig. 8D).

Ingenuity pathway analysis identified Acute Myeloid Leukemia Signature (AMLS) as the most regulated canonical pathway followed by Role of Pattern Recognition Receptors (RPRR) and NFKB (Fig. 8E and Fig. S9A). The AMLS pathway was significantly activated in UPS compared to CTL and LB. Some examples of differentially regulated AMLS genes include *Kitl, Pik3b, Pik3r, Mtor* (Fig. S9A). Similarly, the RPRR pathway was uniquely activated in UPS compared to CTL and LB, with no indication for activation in LB (Fig. 8F). Specific examples of RPRR genes activated by UPS include *Tlr7, Tlr4, Nlrp3, Pik3cb, Il18, C1qc, C1qa, Tgfβ1* (Fig. S9A) but with some genes in this pathway showing reduced expression in UPS (*Il1β, Il1 a., Tlr2*). Activation of NFKB was implicated in the upregulation of many of the genes listed in the RPRR canonical pathway (Fig. S9A). The top upstream regulators were JUN and CEPB which were upregulated in LB compared to CTL and UPS but not between UPS and CTL (Fig. 8G and Fig. S9B). Micro-RNA pathways activity especially let-7a-5p and SPI1/PU.1 transcription factor were downregulated in both LB and UPS (Fig. 8G and Fig. S9B). Overall, the Nanostring findings highlighted significant differences between LB and UPS microglia, several of which involve genes that promote synaptic pruning.

3.9. UPS increases c-fos expression in CA pyramidal neurons

Since UPS involves placing pups in a novel environment, we predicted increased neuronal activation in the Cornu Ammonis (CA) region of P17 UPS pups. Indeed, using c-fos mapping we found a significant effect of rearing on the total number of c-fos positive cells in the CA region that included CA1, CA2, and CA3 ($F(2, 29) = 31.28$, $P < 0.0001$, Fig. 9A–B), with no significant effect of sex ($F(1, 29) = 0.036$, $P = 0.85$) or interaction ($F(2, 29) = 0.29$, $P = 0.75$). Post-hoc analysis confirmed increase c-fos in UPS compared to CTL ($P = <0.0001$) and LB ($P = <0.0001$) with no difference between CTL and LB ($P = 0.98$, Fig. 9). No significant correlation was found between the number of c-fos-positive cells and peripheral levels of corticosterone ($r = 0.11$, $P = 0.78$, $n = 31$) suggesting that the increase in neuronal activation is not likely to be mediated by stress. Given that microglia are highly responsive to ATP gradients released by active synapses (Eyo et al., 2014; Illes et al., 2020), such neuronal activation might promote the increase in microglia ramification, synaptic engulfment and gene expression pattern seen in UPS pups.

4. Discussion

Microglia, the resident innate immune cells in the brain, play a central role in several aspects of circuit development including, neurogenesis, apoptosis, axonal growth, synaptogenesis, synaptic pruning, myelination and inflammation (Borst et al., 2021; Hammond et al., 2021; Johnson and Kaffman, 2018). Microglia are highly sensitive to multiple environmental changes, including mediators of threat and sensory deprivation (Faust et al., 2021; Johnson and Kaffman, 2018). Moreover, transient perturbation in microglial function during the postnatal period leads to long-term changes in myelination (Hagemeyer et al., 2017; Li et al., 2019; Nemes-Baran et al., 2020; Wlodarczyk et al., 2017), connectivity (Bolton et al., 2022; Filipello et al., 2018; Zhan et al., 2014), and behavior (Bolton et al., 2022; Filipello et al., 2018; Lenz et al., 2013; Nelson and Lenz, 2017; Schalbetter et al., 2022; Zhan et al., 2014). These properties led us to suggest that perturbation in microglial function during the

postnatal period contributes to the broad and lasting structural, behavioral and cognitive changes seen in individuals exposed to ELS (Johnson and Kaffman, 2018). Although important progress has been made recently in clarifying some of the mechanisms by which LB impairs synaptic pruning in the developing hypothalamus (Bolton et al., 2022), many details are yet to be clarified. For example, the molecular signals that regulate microglial gene expression and function in response to ELS are yet to be clarified. It is also unclear whether similar mechanisms operate in different types of early adversities and in different brain regions and how sex moderates these outcomes. Finally, exactly how changes in synaptic pruning early in life alter function of circuits that regulate threat detection and cognition later in life is unclear.

This work provides several new insights into the mechanisms by which dysregulation of microglia alters hippocampal development in mice exposed to a single stressor (LB) and multiple unpredictable stressors (UPS). For example, we present compelling evidence that LB and UPS impair synaptic pruning in the developing hippocampus. This assertion is supported by a smaller phagosome compartment as indicated by reduced CD68 staining and less PSD95 puncta inside microglia (Fig. 3). In addition, LB and UPS microglia showed reduced ex vivo phagocytic activity (Fig. 4) and increased spine density in CA1 pyramidal neurons (Fig. 5). Abnormal synaptic pruning during this critical period leads to reduced synaptic strength in the Schaffer collaterals and abnormal connectivity with other brain regions, including the prefrontal cortex later in life (Filipello et al., 2018; Zhan et al., 2014), raising the possibility that abnormal synaptic pruning may contribute to the long-term deficits in hippocampal- dependent learning and connectivity seen in LB and UPS mice (Rocha et al., 2021; White et al., 2020).

During the first two weeks of life, microglia undergo significant morphological changes that include enhanced ramification, a process that is thought to facilitate synaptic pruning (Johnson and Kaffman, 2018; Okajima and Tsuruta, 2018; Zusso et al., 2012). Here we extend previous work showing that this process is significantly impaired in LB mice (Hoeijmakers et al., 2017; Johnson et al., 2018) by directly linking it to impaired capacity to engulf synaptic material. We show that microglial ramification is not correlated with body weight but have not examined the relationship between microglial ramification and hippocampus volume. The observation that microglial ramification is increased in UPS compared to LB mice, suggests that this process is responsive to early adversities that map along the deprivation/enrichment axis (Fig. S1). UPS increases neuronal activation in the developing hippocampus and microglia are highly responsive to ATP gradients released by active synapses (Eyo et al., 2014; Illes et al., 2020), supporting the notion that microglial morphology and function closely track levels of neuronal activation in the developing hippocampus. It would be interesting to test whether chemogenetic activation of CA neurons in the developing hippocampus can mimic changes seen in UPS mice and whether adding toys to LB cages during the second week of life can also enhance microglial ramification and synaptic engulfment. We do not believe that elevated corticosterone is responsible for these changes because corticosterone levels were slightly higher in LB compared to CTL (Fig. 1) and there was no correlation between levels of c-fos activation and peripheral corticosterone levels.

The reduced phagocytic activity seen in the purified ex vivo system demonstrates that LB and UPS directly impair microglial function. We suggest that this impairment is partly mediated by reduced TREM2 surface expression. TREM2 recognizes and facilitates the elimination of non-functional synapses tagged with the “eat me signal” phosphatidylserine (Filipello et al., 2018; Scott-Hewitt et al., 2020) and its levels are reduced on the surface of LB and UPS microglia, in both males and females (Fig. 6A–B). In addition, TREM2 knockout mice share several similarities with LB or UPS mice, including reduced capacity to engulf synaptic material in vivo and ex vivo and increased spine density in CA1 pyramidal neurons (Filipello et al., 2018; Scott-Hewitt et al., 2020). We have confirmed and extended these previous findings by showing that *Trem2* deletion causes a dose-dependent impairment in our ex vivo phagocytic assay (Fig. 7A–B). *Trem2* deletion also reduced total cell volume, phagosome size, and the number of PSD95 puncta inside microglia in the hippocampus of 17-day-old pups (e.g., WT > Hets > Ko, Fig. 8 C–G). However, unlike LB and UPS microglia that display minimal ramification and short processes (Figs. 2–3), *Trem2* ko microglia have numerous long and thin processes, suggesting that other genes are likely to contribute to the morphological and functional changes seen in LB and UPS microglia.

Trem2 mRNA levels were not affected by LB or UPS suggesting an important post-transcriptional regulation of TREM2 activity in the developing hippocampus. Possible mechanisms include membrane trafficking (Yin et al., 2016), changes in micro-RNA levels that regulate TREM2 protein expression (Bhattacharjee et al., 2016), or cleavage by alpha secretases such as ADAM10 and ADAM17 (Schlepckow et al., 2020). Given the critical role that TREM2 plays in guiding normal synaptic pruning, connectivity, and social behavior (Filipello et al., 2018; Scott-Hewitt et al., 2020), it will be important to clarify the mechanisms that govern its surface expression and contribution to connectivity in the dorsal and ventral hippocampus of mice exposed to ELS.

Despite overall similarities between LB and UPS, there are also substantial differences between the two paradigms. This was most notable in the large number of DRG between LB and UPS (about 19 % of all expressed transcripts, Fig. 7A). In fact, LB and UPS showed a greater number of DRG compared to LB-CTL (56DRG) and UPS-CTL (78 DRG), indicating substantial genomic changes between these two paradigms. More specifically, expression of several genes that are known to promote synaptic pruning were elevated in UPS compared to LB (Fig. 6F and 8C). These include increased levels of the complement *C1q* transcripts (e.g. *C1qa, C1qb*, and *C1qc*) which are essential for synaptic pruning (Schafer and Stevens, 2015; Wilton et al., 2019). *Mertk* mRNA levels were also elevated in UPS microglia. MERTK is a receptor that binds to “eat me signals” such as phosphatidylserine (Tung et al., 2013; Wu et al., 2005) and is necessary for synaptic pruning (Bolton et al., 2022) and the removal of apoptotic cells and (Fourgeaud et al., 2016). Levels of the mRNA receptor *Sirp α* which recognizes the “do not eat me signal” CD47 (Lehrman et al., 2018) were also elevated in UPS compared to LB mice. Additional work is needed to confirm similar changes at the protein level and to clarify their contribution to the increase in microglial volume and synaptic engulfment seen in UPS compared to LB mice.

UPS also differed from LB in the mRNA levels of several neurotrophic factors and cytokines that play an essential role in synaptic development and hippocampal function (Fig. 8D). For

example, increased *Tnf* levels seen in LB microglia compared to UPS or CTL conditions, may reduce long-term potentiation and exacerbate hippocampal-dependent deficits (Park and Bowers, 2010). Similarly, reduced nerve growth factor (*Ngf*) levels in LB microglia may further impair synaptic development and normal cognitive development in LB mice (Berry et al., 2012). Exposure to UPS reduced *Il1-β* and Il1- α mRNA levels compared to LB and controls, changes that may alter neurogenesis, neuronal differentiation, synaptic transmission, and the expression of other neurotrophic factors such as NGF and BDNF (Howard, 2013; Liu and Quan, 2018). *Bdnf* mRNA was not detected in any of our groups (less than 20 counts in 50,000 cells) suggesting that it is not expressed at physiological levels in postnatal hippocampal microglia.

Interestingly, CX3CR1 protein surface expression was highest in UPS, followed by significantly reduced levels in LB and further reduction in control condition (Fig. 6F). Given that this receptor plays an essential role in promoting synaptic pruning in the hippocampus (Paolicelli et al., 2011; Zhan et al., 2014), such an increase may represent a compensatory mechanism that helps restore normal synaptic pruning in LB and UPS. Despite these differences, we found a similar increase in spine density in CA1 pyramidal neurons of LB and UPS at P17 and P29 suggesting that these changes may not be sufficient to alter synaptic pruning. However, it is possible that the Golgi staining is not sensitive enough to detect subtle changes in synaptic pruning or that these changes target presynaptic terminals, extra-cellular matrix, or other cell population. Examining the effects of LB and UPS on presynaptic elements is particularly important given recent work showing that they are the primary target for microglial mediated trogocytosis in the developing hippocampus (Weinhard et al., 2018).

A growing body of work has found important sex differences in microglial response to environmental challenges including stress (Han et al., 2021). This was not the case in our study, where males and females' microglia showed similar responses to LB and UPS including morphological changes, in vivo phagocytic activity, receptor levels, spine density and gene expression. There were, however, some interesting differences between the sexes. For example, UPS females showed less pronounced impairment ex vivo phagocytic activity and levels of CD11b/complement 3-receptor were reduced in males LB and UPS but not in females. The sex-specific effects on the CD11b/complement 3-receptor are interesting because this receptor has been shown to play an important role in synaptic pruning in the hippocampus (Schafer et al., 2012). This finding might contribute to abnormal synaptic pruning in males, but is not likely to explain the deficits seen in the ex vivo phagocytic activity and spine density in females exposed to LB and UPS. We suggest that additional sex differences will emerge during puberty when levels of sex hormones and sexual dimorphisms begin to emerge.

The increase in spine density seen in P29 mice is reminiscent of a recent work showing that LB impairs microglial-mediated synaptic pruning in CRH-positive neurons in the developing hypothalamus and that transient perturbation of this process leads to the retention of large numbers of excitatory inputs on CRH neurons that persist later in life (Bolton et al., 2022). Moreover, increased spine density was also reported in the basolateral amygdala (Guadagno et al., 2018) and striatum (He et al., 2021) of LB mice. The only publication that examined

the effects of LB on spine density in CA1 neurons found no differences between LB and CTL mice (Wang et al., 2011). However, Wang et al. (2011) used a shorter exposure to LB (P2-9), a different strain of mice (P2-P9, 129S2/Sv X C57BL/6J mixed background), and assessed spine density in 7-month old mice, making it difficult to compare their finding to those reported here. Similarly, we were unable to replicate previous work showing that exposure to LB reduces dendritic arborization in CA1 pyramidal neurons (Bolton et al., 2020; Brunson et al., 2005; Ivy et al., 2010; Molet et al., 2016). However, this finding was seen in adult rats and to the best of our knowledge has not been replicated yet in mice.

We propose that abnormal synaptic pruning is at least partly responsible for this increase in spine density, but cannot rule out the possibility that increased synaptogenesis may also play a role. A more detailed analysis of spine morphology is needed to determine the type of spines increased in LB and UPS (e.g., thin/filopodia vs mushroom) and whether this increase in spine density facilitates or impairs hippocampal-dependent memory. It is conceivable that the retention of non-functional synapses leads to less efficient network performance, as suggested for some forms of autism spectrum disorders (Faust et al., 2021). However, it is also possible that this increase in spine density represents a compensatory mechanism that aims to reduce the cognitive deficits associated with LB and UPS. Additional work is therefore needed to clarify these issues.

5. Conclusions

Exposure to LB and UPS impairs the ability of microglia to phagocytose synaptic material during a period of intense synaptic pruning in the developing hippocampus. This impairment is mediated by reduced microglial ramification and lower expression of the TREM2 protein. Abnormal synaptic pruning is associated with increased spine density in CA1 pyramidal neurons that persists in juvenile mice that are no longer exposed to stress. These findings suggest that abnormal synaptic pruning during a critical period of hippocampal development may contribute to the long-term hippocampal deficits seen in mice exposed to LB or UPS. Surprisingly, we found that exposure to LB causes more severe impairment in microglial ramification and synaptic engulfment compared to UPS, changes that were accompanied by increase in the expression of several genes that promote synaptic pruning in UPS mice. These findings do not support the cumulative risk factor model and argue that multiple stressors do not necessarily lead to more severe developmental outcomes. Instead, we propose that LB represents a more severe form of early deprivation compared to UPS and that sparse sensory and cognitive stimulation during the second and third weeks of life causes significant deficits in microglial-mediated synaptic pruning in the developing hippocampus.

Supplementary Material

Refer to Web version on PubMed Central for supplementary material.

Acknowledgements

This work was supported by: NIMH R01MH119164, NIMH R01MH118332, and the Clinical Neuroscience Division of the VA National Center for PTSD.

Data availability

Access for genomic work is available in the method section 2.12

References

Anda RF, Felitti VJ, Bremner JD, Walker JD, Whitfield C, Perry BD, Dube SR, Giles WH, 2006. The enduring effects of abuse and related adverse experiences in childhood. A convergence of evidence from neurobiology and epidemiology. Eur. Arch. Psychiatry Clin. Neurosci 256, 174–186. [PubMed: 16311898]

Berry A, Bindocci E, Alleva E, 2012. NGF, brain and behavioral plasticity. Neural Plast. 2012, 784040. [PubMed: 22474604]

Bhattacharjee S, Zhao Y, Dua P, Rogaev EI, Lukiw WJ, 2016. microRNA-34a-mediated down-regulation of the microglial-enriched triggering receptor and phagocytosis-sensor TREM2 in age-related macular degeneration. PLoS ONE 11, e0150211. [PubMed: 26949937]

Bolton JL, Molet J, Ivy A, Baram TZ, 2017. New insights into early-life stress and behavioral outcomes. Curr. Opin. Behav. Sci 14, 133–139. [PubMed: 28413813]

Bolton JL, Schulmann A, Garcia-Curran MM, Regev L, Chen Y, Kamei N, Shao M, Singh-Taylor A, Jiang S, Noam Y, Molet J, Mortazavi A, Baram TZ, 2020. Unexpected transcriptional programs contribute to hippocampal memory deficits and neuronal stunting after early-life adversity. Cell Rep. 33, 108511. [PubMed: 33326786]

Bolton JL, Short AK, Othy S, Kooiker CL, Shao M, Gunn BG, Beck J, Bai X, Law SM, Savage JC, Lambert JJ, Belelli D, Tremblay ME, Cahalan MD, Baram TZ, 2022. Early stress-induced impaired microglial pruning of excitatory synapses on immature CRH-expressing neurons provokes aberrant adult stress responses. Cell Rep. 38, 110600. [PubMed: 35354026]

Borst K, Dumas AA, Prinz M, 2021. Microglia: Immune and non-immune functions. Immunity 54, 2194–2208. [PubMed: 34644556]

Brunson KL, Kramar E, Lin B, Chen Y, Colgin LL, Yanagihara TK, Lynch G, Baram TZ, 2005. Mechanisms of late-onset cognitive decline after early-life stress. J. Neurosci 25, 9328–9338. [PubMed: 16221841]

Chen LP, Murad MH, Paras ML, Colbenson KM, Sattler AL, Goranson EN, Elamin MB, Seime RJ, Shinozaki G, Prokop LJ, Zirakzadeh A, 2010. Sexual abuse and lifetime diagnosis of psychiatric disorders: systematic review and meta-analysis. Mayo Clin. Proc 85, 618–629. [PubMed: 20458101]

Delpech JC, Wei L, Hao J, Yu X, Madore C, Butovsky O, Kaffman A, 2016. Early life stress perturbs the maturation of microglia in the developing hippocampus. Brain Behav. Immunity

Evans GW, Li D, Whipple SS, 2013. Cumulative risk and child development. Psychol. Bull 139, 1342–1396. [PubMed: 23566018]

Eyo UB, Peng J, Swiatkowski P, Mukherjee A, Bispo A, Wu LJ, 2014. Neuronal hyperactivity recruits microglial processes via neuronal NMDA receptors and microglial P2Y12 receptors after status epilepticus. J. Neurosci 34, 10528–10540. [PubMed: 25100587]

Faust TE, Gunner G, Schafer DP, 2021. Mechanisms governing activity-dependent synaptic pruning in the developing mammalian CNS. Nat. Rev. Neurosci 22, 657–673. [PubMed: 34545240]

Favuzzi E, Huang S, Saldi GA, Binan L, Ibrahim LA, Fernandez-Otero M, Cao Y, Zeine A, Sefah A, Zheng K, Xu Q, Khlestova E, Farhi SL, Bonneau R, Datta SR, Stevens B, Fishell G, 2021. GABA-receptive microglia selectively sculpt developing inhibitory circuits. Cell 184 (4048-4063), e4032.

Filipello F, Morini R, Corradini I, Zerbi V, Canzi A, Michalski B, Erreni M, Markicevic M, Starvaggi-Cucuzza C, Otero K, Piccio L, Cignarella F, Perrucci F, Tamborini M, Genua M, Rajendran L, Menna E, Vetrano S, Fahnestock M, Paolicelli RC, Matteoli M, 2018. The microglial innate immune receptor TREM2 is required for synapse elimination and normal brain connectivity. Immunity 48 (979-991), e978.

Fourgeaud L, Traves PG, Tufail Y, Leal-Bailey H, Lew ED, Burrola PG, Callaway P, Zagorska A, Rothlin CV, Nimmerjahn A, Lemke G, 2016. TAM receptors regulate multiple features of microglial physiology. Nature 532, 240–244. [PubMed: 27049947]

Grossman AW, Aldridge GM, Lee KJ, Zeman MK, Jun CS, Azam HS, Arii T, Imoto K, Greenough WT, Rhyu IJ, 2010. Developmental characteristics of dendritic spines in the dentate gyrus of Fmr1 knockout mice. Brain Res. 1355, 221–227. [PubMed: 20682298]

Guadagno A, Wong TP, Walker CD, 2018. Morphological and functional changes in the preweaning basolateral amygdala induced by early chronic stress associate with anxiety and fear behavior in adult male, but not female rats. Prog. NeuroPsychopharmacol. Biol. Psychiatry 81, 25–37. [PubMed: 28963066]

Hagemeyer N, Hanft KM, Akriditou MA, Unger N, Park ES, Stanley ER, Staszewski O, Dimou L, Prinz M, 2017. Microglia contribute to normal myelinogenesis and to oligodendrocyte progenitor maintenance during adulthood. Acta Neuropathol. 134, 441–458. [PubMed: 28685323]

Hammond BP, Manek R, Kerr BJ, Macauley MS, Plemel JR, 2021. Regulation of microglia population dynamics throughout development, health, and disease. Glia 69, 2771–2797. [PubMed: 34115410]

Han J, Fan Y, Zhou K, Blomgren K, Harris RA, 2021. Uncovering sex differences of rodent microglia. J. Neuroinflamm 18, 74.

He Y, Xu B, Chen Y, Liu L, Xu L, Chen Y, Long D, 2021. Early-life adversity selectively interrupts the dendritic differentiation of dorsolateral striatal neurons in male mice. Brain Struct. Funct 226, 397–414. [PubMed: 33386419]

Hoeijmakers L, Ruigrok SR, Amelianchik A, Ivan D, van Dam AM, Lucassen PJ, Korosi A, 2017. Early-life stress lastingly alters the neuroinflammatory response to amyloid pathology in an Alzheimer's disease mouse model. Brain Behav. Immun 63, 160–175. [PubMed: 28027926]

Howard J, 2013. The cytokine hypothesis: A neurodevelopmental explanation for the emergence of schizophrenia later in life. Adv. Biosci. Biotechnol 4, 81–88.

Illes P, Rubini P, Ulrich H, Zhao Y, Tang Y, 2020. Regulation of microglial functions by purinergic mechanisms in the healthy and diseased CNS. Cells 9.

Ivy AS, Rex CS, Chen Y, Dube C, Maras PM, Grigoriadis DE, Gall CM, Lynch G, Baram TZ, 2010. Hippocampal dysfunction and cognitive impairments provoked by chronic early-life stress involve excessive activation of CRH receptors. J. Neurosci 30, 13005–13015. [PubMed: 20881118]

Johnson FK, Delpech JC, Thompson GJ, Wei L, Hao J, Herman P, Hyder F, Kaffman A, 2018. Amygdala hyper-connectivity in a mouse model of unpredictable early life stress. Transl. Psychiatry 8, 49. [PubMed: 29463821]

Johnson FK, Kaffman A, 2018. Early life stress perturbs the function of microglia in the developing rodent brain: New insights and future challenges. Brain Behav. Immun 69, 18–27. [PubMed: 28625767]

Kaffman A, Meaney MJ, 2007. Neurodevelopmental sequelae of postnatal maternal care in rodents: clinical and research implications of molecular insights. J. Child Psychol. Psychiatry 48, 224–244. [PubMed: 17355397]

Kessler RC, Davis CG, Kendler KS, 1997. Childhood adversity and adult psychiatric disorder in the US National Comorbidity Survey. Psychol. Med 27, 1101–1119. [PubMed: 9300515]

Kuhn CM, Schanberg SM, 1998. Responses to maternal separation: mechanisms and mediators. Int. J. Dev. Neurosci 16, 261–270. [PubMed: 9785122]

Lehrman EK, Wilton DK, Litvina EY, Welsh CA, Chang ST, Frouin A, Walker AJ, Heller MD, Umemori H, Chen C, Stevens B, 2018. CD47 Protects Synapses from Excess Microglia-Mediated Pruning during Development. Neuron 100 (120–134), e126.

Lenz KM, Nugent BM, Haliyur R, McCarthy MM, 2013. Microglia are essential to masculinization of brain and behavior. J. Neurosci 33, 2761–2772. [PubMed: 23407936]

Li Q, Cheng Z, Zhou L, Darmanis S, Neff NF, Okamoto J, Gulati G, Bennett ML, Sun LO, Clarke LE, Marschallinger J, Yu G, Quake SR, Wyss-Coray T, Barres BA, 2019. Developmental heterogeneity of microglia and brain myeloid cells revealed by deep single-cell RNA sequencing. Neuron 101 (207–223), e210.

Liu X, Quan N, 2018. Microglia and CNS Interleukin-1: Beyond Immunological Concepts. Front. Neurol 9, 8. [PubMed: 29410649]

McLaughlin KA, Colich NL, Rodman AM, Weissman DG, 2020. Mechanisms linking childhood trauma exposure and psychopathology: a transdiagnostic model of risk and resilience. BMC Med. 18, 96. [PubMed: 32238167]

McLaughlin KA, Sheridan MA, 2016. Beyond cumulative risk: A dimensional approach to childhood adversity. Curr. Direct. Psychol. Sci 25, 239–245.

McLaughlin KA, Sheridan MA, Lambert HK, 2014. Childhood adversity and neural development: deprivation and threat as distinct dimensions of early experience. Neurosci. Biobehav. Rev 47, 578–591. [PubMed: 25454359]

Molet J, Maras PM, Kinney-Lang E, Harris NG, Rashid F, Ivy AS, Solodkin A, Obenaus A, Baram TZ, 2016. MRI uncovers disrupted hippocampal microstructure that underlies memory impairments after early-life adversity. Hippocampus 26, 1618–1632. [PubMed: 27657911]

Nelson LH, Lenz KM, 2017. Microglia depletion in early life programs persistent changes in social, mood-related, and locomotor behavior in male and female rats. Behav. Brain Res 316, 279–293. [PubMed: 27613230]

Nemes-Baran AD, White DR, DeSilva TM, 2020. Fractalkine-dependent microglial pruning of viable oligodendrocyte progenitor cells regulates myelination. Cell Rep. 32, 108047. [PubMed: 32814050]

Okajima T, Tsuruta F, 2018. Microglial dynamics during brain development. Neural Regener. Res 13, 222–223.

Orso R, Creutzberg KC, Kestering-Ferreira E, Wearick-Silva LE, Tractenberg SG, Grassi-Oliveira R, 2020. Maternal separation combined with limited bedding increases anxiety-like behavior and alters hypothalamic-pituitary-adrenal axis function of male BALB/cJ mice. Front. Behav. Neurosci

Paolicelli RC, Bolasco G, Pagani F, Maggi L, Scianni M, Panzanelli P, Giustetto M, Ferreira TA, Guiducci E, Dumas L, Ragozzino D, Gross CT, 2011. Synaptic pruning by microglia is necessary for normal brain development. Science 333, 1456–1458. [PubMed: 21778362]

Paolicelli RC, Bolasco G, Pagani F, Maggi L, Scianni M, Panzanelli P, Giustetto M, Ferreira TA, Guiducci E, Dumas L, Ragozzino D, Gross CT, Synaptic pruning by microglia is necessary for normal brain development. Science 333, 1456–1458.

Park KM, Bowers WJ, 2010. Tumor necrosis factor-alpha mediated signaling in neuronal homeostasis and dysfunction. Cell. Signal 22, 977–983. [PubMed: 20096353]

Peterson C, Florence C, Klevens J, 2018. The economic burden of child maltreatment in the United States, 2015. Child Abuse Negl. 86, 178–183. [PubMed: 30308348]

Rocha M, Wang D, Avila-Quintero V, Bloch MH, Kaffman A, 2021. Deficits in hippocampal-dependent memory across different rodent models of early life stress: systematic review and meta-analysis. Transl. Psychiatry 11, 231. [PubMed: 33879774]

Schafer DP, Lehrman EK, Kautzman AG, Koyama R, Mardinly AR, Yamasaki R, Ransohoff RM, Greenberg ME, Barres BA, Stevens B, 2012. Microglia sculpt postnatal neural circuits in an activity and complement-dependent manner. Neuron 74, 691–705. [PubMed: 22632727]

Schafer DP, Stevens B, 2015. Microglia function in central nervous system development and plasticity. Cold Spring Harb. Perspect. Biol 7, a020545. [PubMed: 26187728]

Schalbetter SM, von Arx AS, Cruz-Ochoa N, Dawson K, Ivanov A, Mueller FS, Lin HY, Amport R, Mildenberger W, Mattei D, Beule D, Foldy C, Greter M, Notter T, Meyer U, 2022. Adolescence is a sensitive period for prefrontal microglia to act on cognitive development. Sci. Adv 8, eabi6672. [PubMed: 35235358]

Schlepckow K, Monroe KM, Kleinberger G, Cantuti-Castelvetri L, Parhizkar S, Xia D, Willem M, Werner G, Pettkus N, Brunner B, Sulzen A, Nuscher B, Hampel H, Xiang X, Feederle R, Tahirovic S, Park JI, Prorok R, Mahon C, Liang CC, Shi J, Kim DJ, Sabelstrom H, Huang F, Di Paolo G, Simons M, Lewcock JW, Haass C, 2020. Enhancing protective microglial activities with a dual function TREM2 antibody to the stalk region. EMBO Mol. Med 12, e11227. [PubMed: 32154671]

Scott-Hewitt N, Perrucci F, Morini R, Erreni M, Mahoney M, Witkowska A, Carey A, Faggiani E, Schuetz LT, Mason S, Tamborini M, Bizzotto M, Passoni L, Filipello F, Jahn R, Stevens B, Matteoli M, 2020. Local externalization of phosphatidylserine mediates developmental synaptic pruning by microglia. EMBO J. 39, e105380. [PubMed: 32657463]

Teicher MH, Samson JA, 2016. Annual Research Review: Enduring neurobiological effects of childhood abuse and neglect. J. Child Psychol. Psychiatry 57, 241–266. [PubMed: 26831814]

Tung TT, Nagaosa K, Fujita Y, Kita A, Mori H, Okada R, Nonaka S, Nakanishi Y, 2013. Phosphatidylserine recognition and induction of apoptotic cell clearance by Drosophila engulfment receptor Draper. J. Biochem 153, 483–491. [PubMed: 23420848]

Walker CD, Bath KG, Joels M, Korosi A, Larauche M, Lucassen PJ, Morris MJ, Raineki C, Roth TL, Sullivan RM, Tache Y, Baram TZ, 2017. Chronic early life stress induced by limited bedding and nesting (LBN) material in rodents: critical considerations of methodology, outcomes and translational potential. Stress 20, 421–448. [PubMed: 28617197]

Wang XD, Rammes G, Kraev I, Wolf M, Liebl C, Scharf SH, Rice CJ, Wurst W, Holsboer F, Deussing JM, Baram TZ, Stewart MG, Muller MB, Schmidt MV, 2011. Forebrain CRF(1) modulates early-life stress-programmed cognitive deficits. J. Neurosci 31, 13625–13634. [PubMed: 21940453]

Wei L, Simen A, Mane S, Kaffman A, 2012. Early life stress inhibits expression of a novel innate immune pathway in the developing hippocampus. Neuropsychopharmacology 37, 567–580. [PubMed: 21993208]

Wei L, Hao J, Lacher RK, Abbott T, Chung L, Colangelo CM, Kaffman A, 2015. Early-life stress perturbs key cellular programs in the developing mouse hippocampus. Dev. Neurosci

Weinhard L, di Bartolomei G, Bolasco G, Machado P, Schieber NL, Neniskyte U, Exiga M, Vadisiute A, Raggioli A, Schertel A, Schwab Y, Gross CT, 2018. Microglia remodel synapses by presynaptic trogocytosis and spine head filopodia induction. Nat. Commun 9, 1228. [PubMed: 29581545]

White JD, Kaffman A, 2019. The moderating effects of sex on consequences of childhood maltreatment: from clinical studies to animal models. Front. Neurosci 13, 1082. [PubMed: 31680821]

White JD, Arefin TM, Pugliese A, Lee CH, Gassen J, Zhang J, Kaffman A, 2020. Early life stress causes sex-specific changes in adult fronto-limbic connectivity that differentially drive learning. Elife 9.

Wilton DK, Dissing-Olesen L, Stevens B, 2019. Neuron-glia signaling in synapse elimination. Annu. Rev. Neurosci 42, 107–127. [PubMed: 31283900]

Wlodarczyk A, Holtman IR, Krueger M, Yogev N, Bruttger J, Khorooshi R, Benmamar-Badel A, de Boer-Bergsma JJ, Martin NA, Karram K, Kramer I, Boddeke EW, Waisman A, Eggen BJ, Owens T, 2017. A novel microglial subset plays a key role in myelinogenesis in developing brain. EMBO J. 36, 3292–3308. [PubMed: 28963396]

Workman AD, Charvet CJ, Clancy B, Darlington RB, Finlay BL, 2013. Modeling transformations of neurodevelopmental sequences across mammalian species. J. Neurosci 33, 7368–7383. [PubMed: 23616543]

Wu Y, Singh S, Georgescu MM, Birge RB, 2005. A role for Mer tyrosine kinase in alphavbeta5 integrin-mediated phagocytosis of apoptotic cells. J. Cell Sci 118, 539–553. [PubMed: 15673687]

Yin J, Liu X, He Q, Zhou L, Yuan Z, Zhao S, 2016. Vps35-dependent recycling of Trem2 regulates microglial function. Traffic 17, 1286–1296. [PubMed: 27717139]

Zeiss CJ, 2021. Comparative milestones in rodent and human postnatal central nervous system development. Toxicol. Pathol 49, 1368–1373. [PubMed: 34569375]

Zhan Y, Paolicelli RC, Sforazzini F, Weinhard L, Bolasco G, Pagani F, Vyssotski AL, Bifone A, Gozzi A, Ragozzino D, Gross CT, 2014. Deficient neuron-microglia signaling results in impaired functional brain connectivity and social behavior. Nat. Neurosci 17, 400–406. [PubMed: 24487234]

Zusso M, Methot L, Lo R, Greenhalgh AD, David S, Stifani S, 2012. Regulation of postnatal forebrain amoeboid microglial cell proliferation and development by the transcription factor Runx1. J. Neurosci 32, 11285–11298. [PubMed: 22895712]

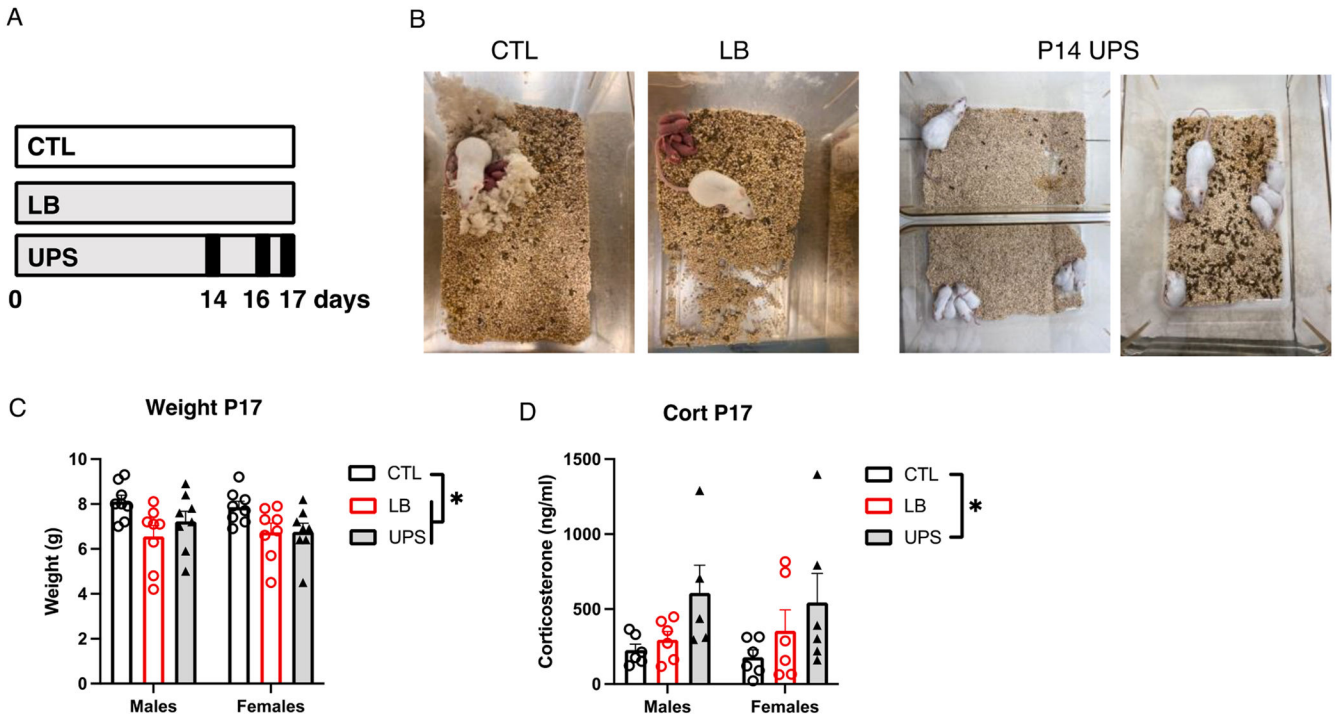

Fig. 1.

UPS increases corticosterone levels in 17-Day old pups. (A) Experimental timeline, with black lines in UPS representing the 3 maternal separation/nest disruption events. (B) Pictures of P2 CTL and LB cages and P14 UPS cage during the first separation and reunion. Effects of rearing and sex on weight (C), and corticosterone levels (D) in 17-day-old pups. N = 8 mice per rearing and sex group for weight and N = 5–6 mice per rearing and sex group for corticosterone. Error bars represent mean ± SEM. *$p < 0.05$.

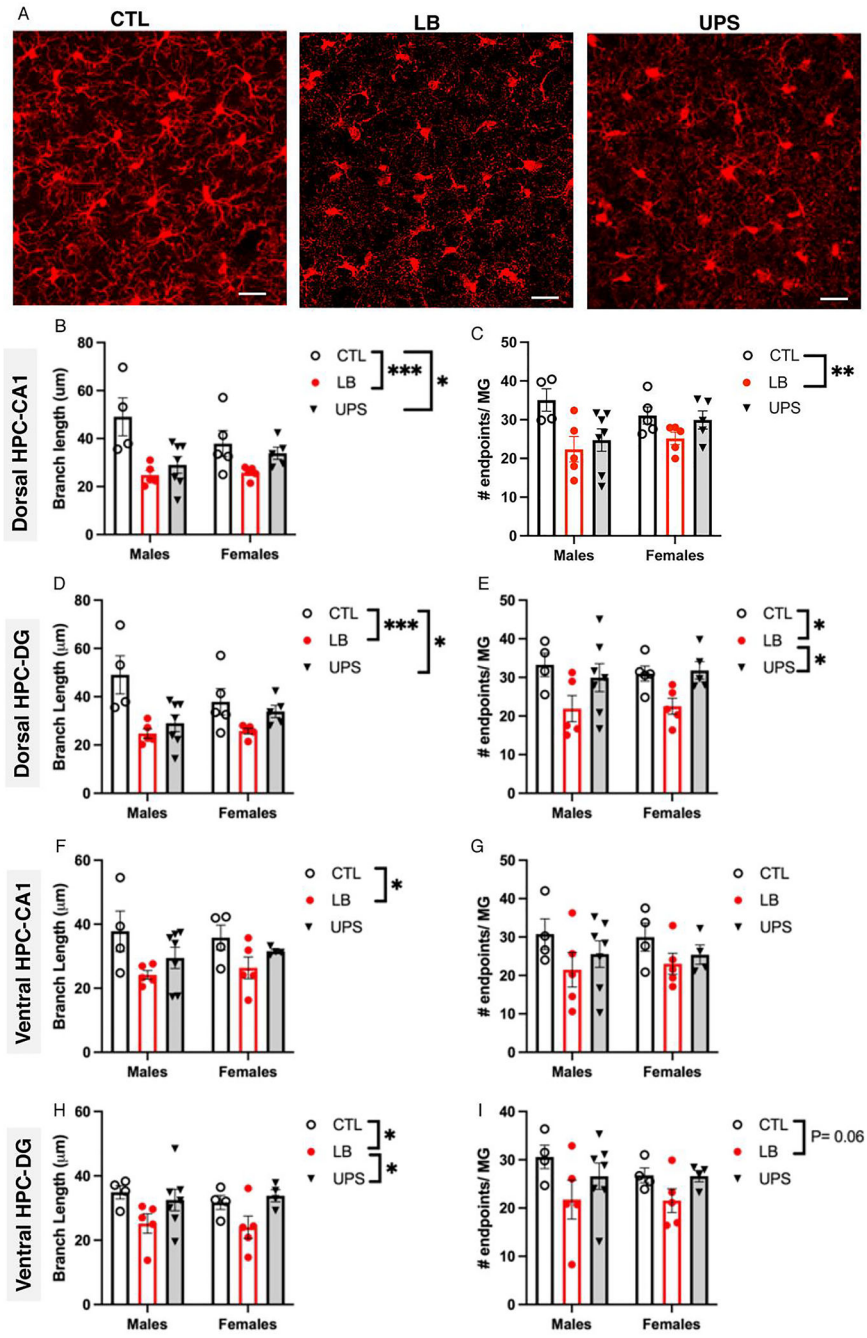

Fig. 2.

Greater reduction in microglial ramification is seen in LB compared to UPS. (A) representative confocal images of Iba1 staining in the dorsal hippocampus of P17 pups exposed to CTL, LB, and UPS. Effects of rearing and sex on microglial branch length (B, D, F, H) and number of branch-endpoints (C, E, G, I) in the dorsal hippocampus CA1 region (B-C), dorsal hippocampus dentate gyrus (D-E), ventral hippocampus CA1 region (F-G), ventral hippocampus dentate gyrus (H-I). N = 4–7 mice per rearing and sex group. Scale bars in A are 20 µm. Error bars represent mean ± SEM. *p < 0.05, **p < 0.01, ***p < 0.001.

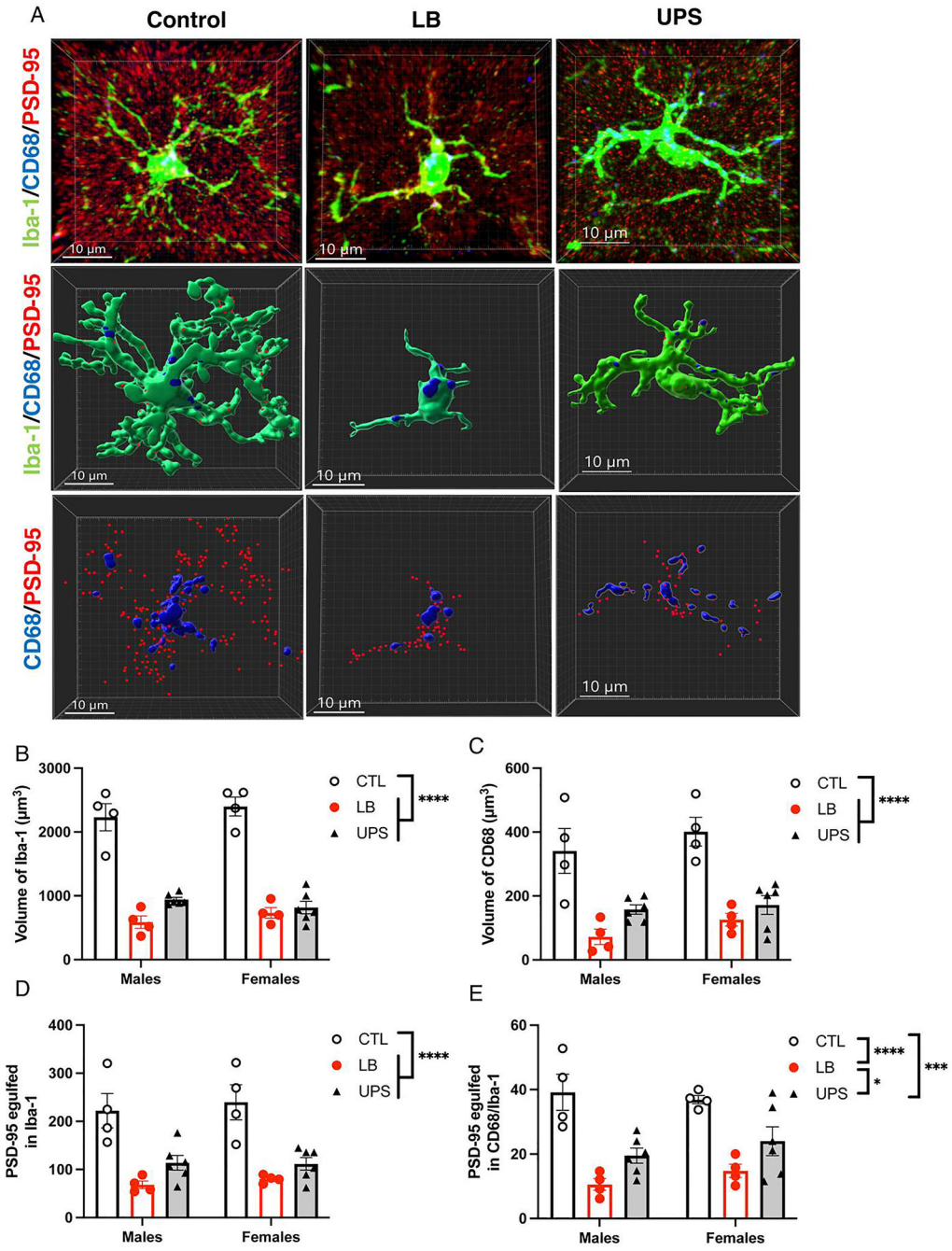

Fig. 3.

ELS impairs the engulfment of synaptic material in vivo. (A) Representative confocal images (top row) and Imaris models (middle and lower rows) of microglia from control, LB, and UPS P17 mice showing staining for Iba1 (green), CD68 (blue), and PSD95 (red). Middle row: reconstruction of Iba1 & CD68 staining. Lower row: reconstruction of CD68 and PSD95 staining inside microglia. Effects of rearing and sex on microglial volume (B), CD68 volume inside microglia (C), PSD95 puncta inside microglia (D), and PSD95 puncta inside CD68 phagosomes (E). N = 4–6 animals (5 cells per animal) per rearing and sex

group (total of 28 mice, 140 cells). Error bars represent mean ± SEM. ****p < 0.0001, ***p < 0.001, *p < 0.05.

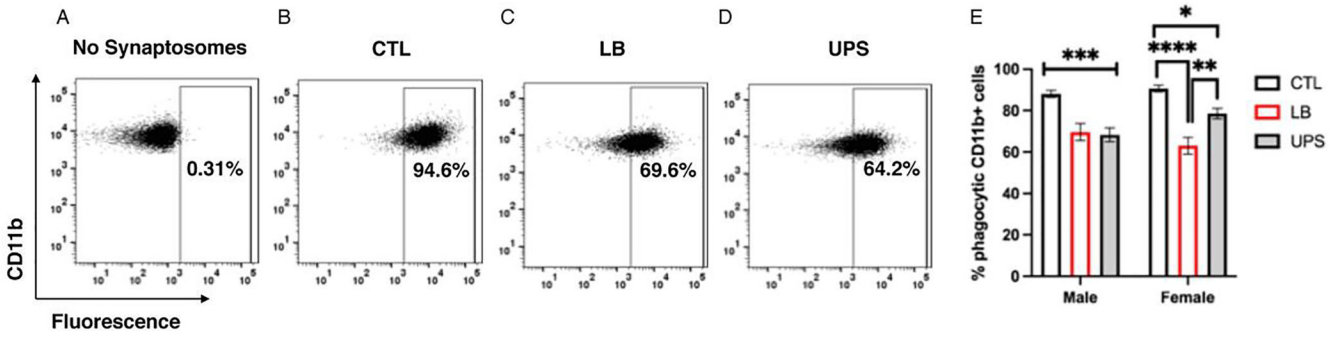

Fig. 4.

ELS impairs phagocytic activity ex vivo. Microglia isolated from the hippocampus of P17 pups were incubated with pHrodo labeled synaptosomes to assess phagocytic activity ex vivo. (A) No synaptosome control used to gate non-phagocytic microglia. Representative scatter plots showing the percentage of fluorescently labeled microglia from CTL (B), LB (C) and UPS (D). (E) Exposure to LB and UPS reduced ex vivo phagocytic activity, an effect that was less pronounced in UPS females. N = 17–22 mice per rearing and sex group. Error bars represent mean ± SEM. *p < 0.05, **p < 0.01, ***p < 0.001, ****p < 0.0001.

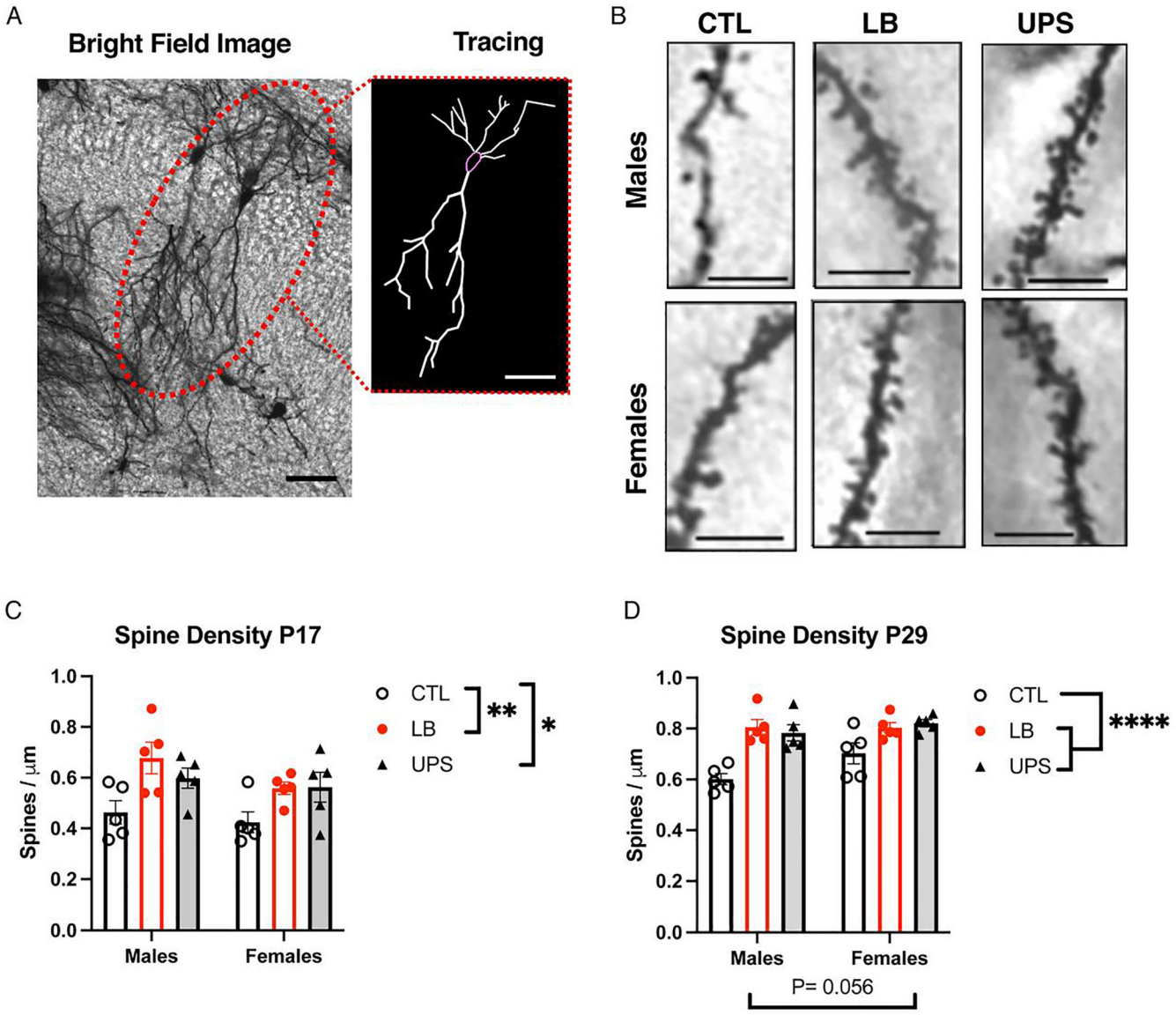

Fig. 5.

ELS increases spine density in CA1 pyramidal neurons in the dorsal hippocampus of P17 and P29 mice. Representative bright field image of Golgi-stained CA1 neurons (A) and apical spines (B) in the dorsal hippocampus with 2-d Neurolucida tracing shown in (A). ELS increased spine density in P17 (C) and P29 (D). N = 5 mice per rearing and sex per age (total of 30 mice per age). Scale bars are 20 µm in A and 5 µm in B. Error bars represent mean ± SEM. *p < 0.05, **p < 0.01, ****p < 0.0001.

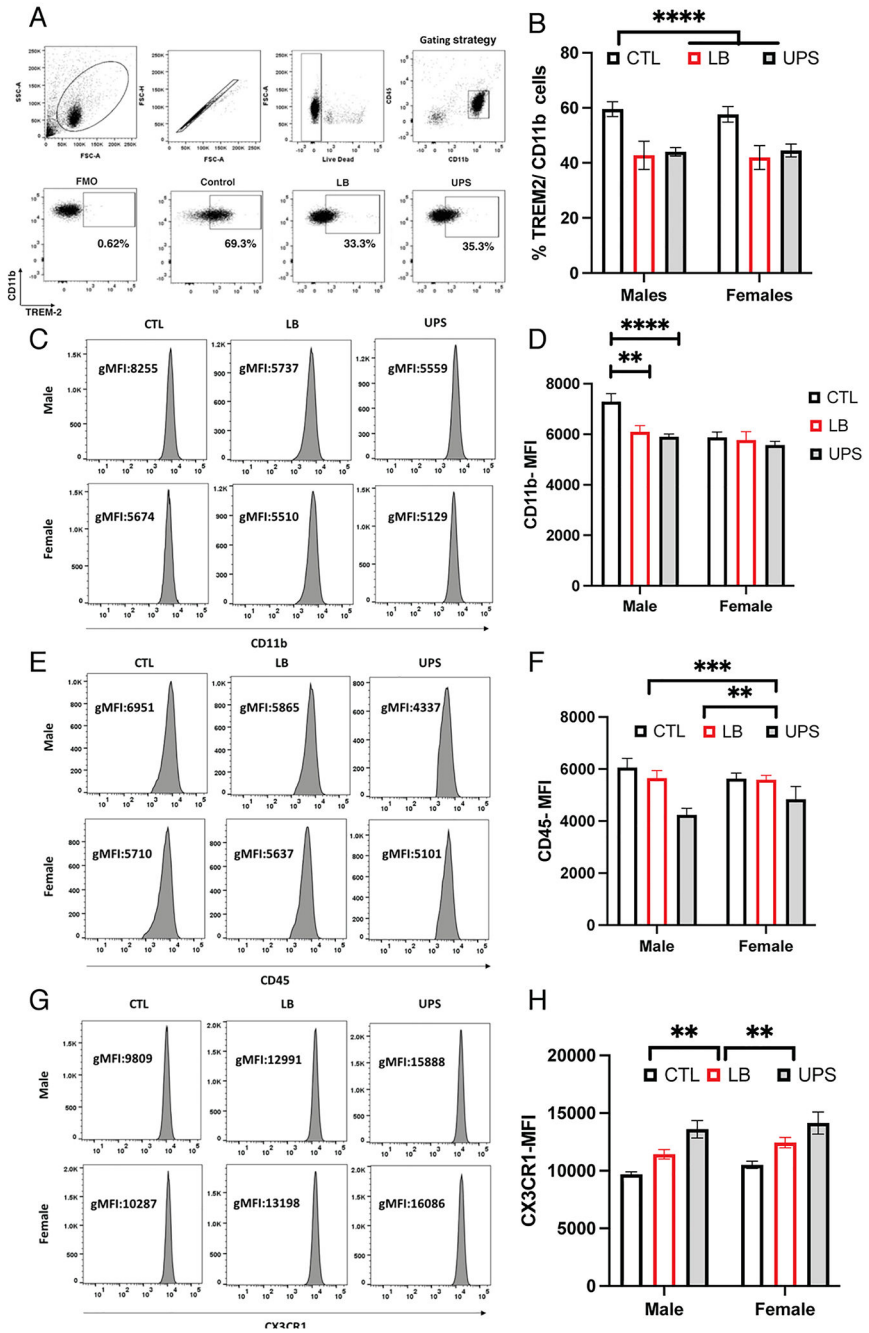

Fig. 6.

ELS reduces expression of TREM2 and CD11b while increasing CX3CR1 in P17 microglia. (A) Scatter plots for quantifying Trem2 positive microglia in CTL, LB and UPS. (B) Percentage of TREM2-positive microglia. Median fluorescence intensity (MFI) plots and surface expression of CD11b (C-D), CD45 (E-F) and CX3CR1 (G-H). CTL-males: n = 16, CTL-females: n = 14, LB males: n = 10, LB-females: n = 9, UPS-males: n = 12, UPS-females: n = 16. Error bars represent mean ± SEM. **p < 0.01, ***p < 0.001, ****p < 0.0001.

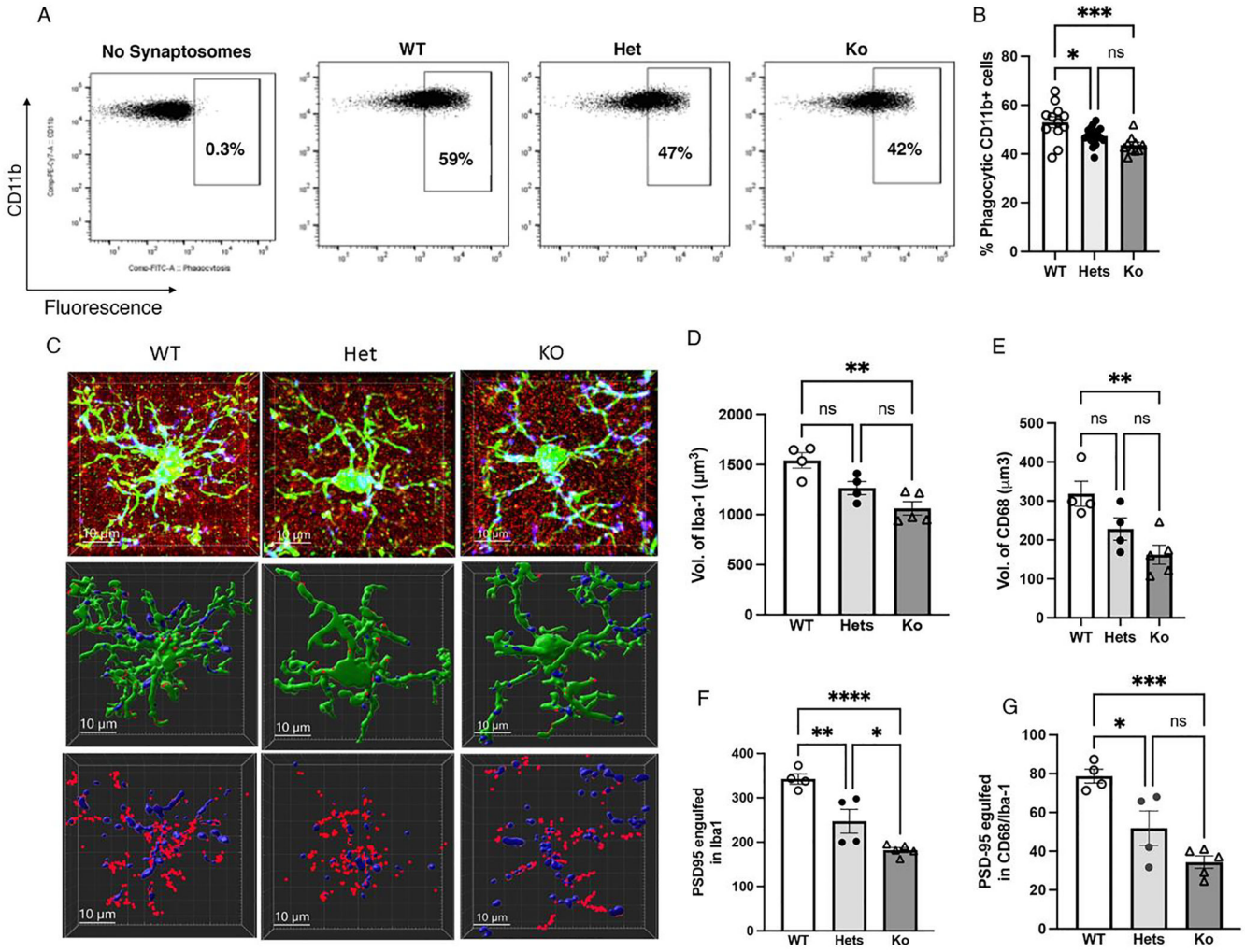

Fig. 7.

Trem2 is essential for normal phagocytic activity. (A-B) Effects of *Trem2* genotype (WT, Hets, Ko) on ex vivo phagocytic activity in microglia isolated from the hippocampus of 17-day old pups (n = 10–17 pups per group, 50 % females). (C) Representative confocal images (top row) and Imaris models (middle and lower rows) of microglia from Trem2 wildtype (WT), heterozygous (Hets) and knockout P17 littermates. Staining for Iba1 (green), CD68 (blue), and PSD95 (red). Middle row: reconstruction of Iba1 & CD68 staining. Lower row: reconstruction of CD68 and PSD95 staining inside microglia. Effects of Trem2 genotype on microglial volume (D), CD68 volume inside microglia (E), number of PSD95 puncta in microglia (F) and PSD95 puncta inside CD68 (G), n = 5 cells per mouse and 4–5 mice per group, 50 % females). Error bars represent mean ± SEM. *p < 0.05, **p < 0.01, ***p < 0.001, ****p < 0.0001.

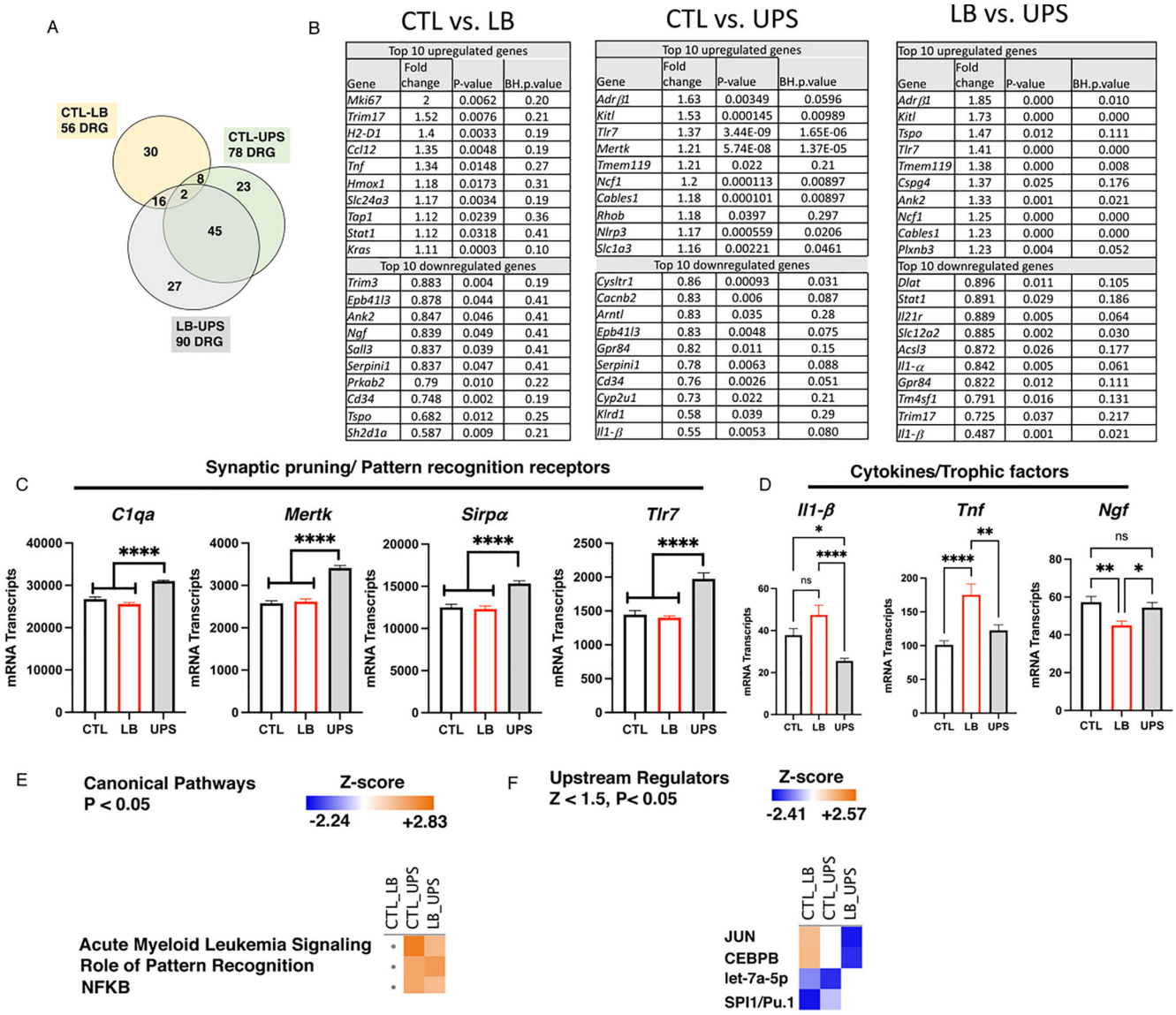

Top 10 upregulated genes

Gene	Fold change	P-value	BH.p.value
Mki67	2	0.0062	0.20
Trim17	1.52	0.0076	0.21
H2-D1	1.4	0.0033	0.19
Ccl12	1.35	0.0048	0.19
Tnf	1.34	0.0148	0.27
Hmox1	1.18	0.0173	0.31
Slc24a3	1.17	0.0034	0.19
Tap1	1.12	0.0239	0.36
Stat1	1.12	0.0318	0.41
Kras	1.11	0.0003	0.10

Top 10 downregulated genes

Gene	Fold change	P-value	BH.p.value
Trim3	0.883	0.004	0.19
Epb41l3	0.878	0.044	0.41
Ank2	0.847	0.046	0.41
Ngf	0.839	0.049	0.41
Sall3	0.837	0.039	0.41
Serpini1	0.837	0.047	0.41
Prkab2	0.79	0.010	0.22
Cd34	0.748	0.002	0.19
Tspo	0.682	0.012	0.25
Sh2d1a	0.587	0.009	0.21

Top 10 upregulated genes

Gene	Fold change	P-value	BH.p.value
Adrβ1	1.63	0.00349	0.0596
Kitl	1.53	0.000145	0.00989
Tlr7	1.37	3.44E-09	1.65E-06
Mertk	1.21	5.74E-08	1.37E-05
Tmem119	1.21	0.022	0.21
Ncf1	1.2	0.000113	0.00897
Cables1	1.18	0.000101	0.00897
Rhob	1.18	0.0397	0.297
Nlrp3	1.17	0.000559	0.0206
Slc1a3	1.16	0.00221	0.0461

Top 10 downregulated genes

Gene	Fold change	P-value	BH.p.value
Cysltr1	0.86	0.00093	0.031
Cacnb2	0.83	0.006	0.087
Arntl	0.83	0.035	0.28
Epb41l3	0.83	0.0048	0.075
Gpr84	0.82	0.011	0.15
Serpini1	0.78	0.0063	0.088
Cd34	0.76	0.0026	0.051
Cyp2u1	0.73	0.022	0.21
Klrd1	0.58	0.039	0.29
Il1-β	0.55	0.0053	0.080

Top 10 upregulated genes

Gene	Fold change	P-value	BH.p.value
Adrβ1	1.85	0.000	0.010
Kitl	1.73	0.000	0.000
Tspo	1.47	0.012	0.111
Tlr7	1.41	0.000	0.000
Tmem119	1.38	0.000	0.008
Cspg4	1.37	0.025	0.176
Ank2	1.33	0.001	0.021
Ncf1	1.25	0.000	0.000
Cables1	1.23	0.000	0.000
Plxnb3	1.23	0.004	0.052

Top 10 downregulated genes

Gene	Fold change	P-value	BH.p.value
Dlat	0.896	0.011	0.105
Stat1	0.891	0.029	0.186
Il21r	0.889	0.005	0.064
Slc12a2	0.885	0.002	0.030
Acsl3	0.872	0.026	0.177
Il1-α	0.842	0.005	0.061
Gpr84	0.822	0.012	0.111
Tm4sf1	0.791	0.016	0.131
Trim17	0.725	0.037	0.217
Il1-β	0.487	0.001	0.021

Fig. 8.

UPS causes distinct transcriptional changes compared to LB and control conditions. (A) Venn diagram showing the number of DRG between CTL, LB and UPS. (B) The top 10 upregulated and down DRG in CTL-LB, CTL-UPS, and LB-UPS comparisons. (C) UPS increases expression of genes implicated in synaptic pruning. (D) Levels of cytokines and neurotrophic factors differentially affected by LB and UPS. Canonical pathway (E) and upstream regulators analyses (F) for the most regulated pathways and transcription factors respectively. Abbreviations: B-H: Benjamini-Hochberg, NFKB: Nuclear Factor kappa-light-chain-enhancer of activated B cells, CEBPB: CCAAT/enhancer binding protein beta.

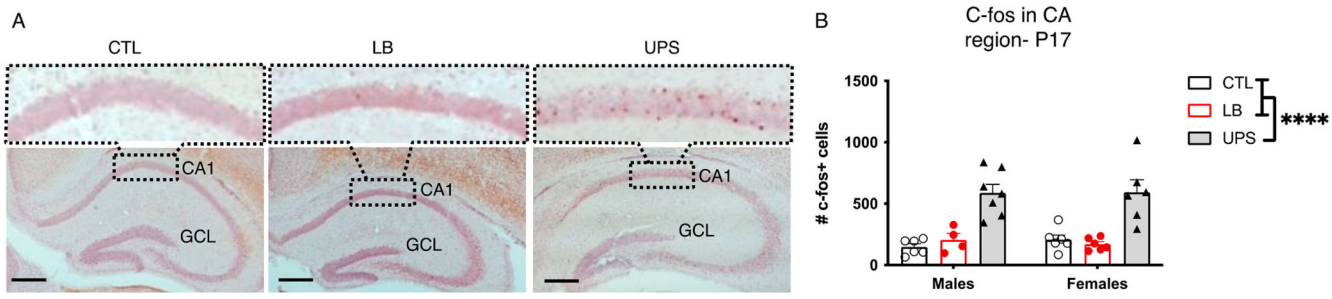

Fig. 9.

UPS Increases c-fos expression in the developing hippocampus. (A) Representative bright field images of c-fos-positive cells in the hippocampus of P17 pups, with higher magnification insert shown on top. (B) Total number of c-fos-positive cells in CA1-3 regions of the hippocampus. N = 4–7 mice per rearing and sex (total of 35 mice). Error bars represent mean ± SEM. ****$p < 0.0001$.